UNIVERSITY OF CALIFORNIA

Los Angeles

Co-production of Acetic Acid and Hydrogen/Power from Natural Gas with Zero Carbon Dioxide Emissions

A thesis submitted in partial satisfaction

of the requirements for the degree Master of Science

in Chemical Engineering

by

Ibubeleye Somiari

2017

ABSTRACT OF THE THESIS

Co-production of Acetic Acid and Hydrogen/Power from Natural Gas

with Zero Carbon Dioxide Emissions

by

Ibubeleye Somiari

Master of Science in Chemical Engineering

University of California, Los Angeles, 2017

Professor Vasilios Manousiouthakis, Chair

In this work, a process plant flow sheet that co-produces acetic acid and hydrogen/power from natural gas with zero carbon dioxide emissions is developed. Two cases are explored: the production of acetic acid and hydrogen (case 1) and the production of acetic acid and power (case 2). This is realized by the selection of an appropriate reaction cluster whose sum results in the overall reaction that co-produces acetic acid and hydrogen/power. The concept of energetic self-sufficiency is introduced and it imposes constraints on the system defined in terms of the ratio of oxygen feed to acetic acid produced. Heat and power integration of the converged flowsheet reveals an operating range for each case that guarantees energetic self-sufficiency. Operating points are chosen to conduct a preliminary economic analysis and a carbon dioxide cost and performance metric calculation to quantify profitability and carbon capture potential of the overall process.

The thesis of Ibubeleye Somiari is approved.

Yvonne Chen

Tatiana Segura

Vasilios Manousiouthakis, Committee Chair

University of California, Los Angeles

2017

TABLE OF CONTENTS

LIST OF FIGURES

LIST OF TABLES

LIST OF SYMBOLS

g_i : Specific molar Gibbs free energy of material stream i $\left(kJ/mol\right)$

G_i : Specific mass Gibbs free energy of material stream i $\left(kJ/kg\right)$

h_i : Specific molar enthalpy of material stream i $\left(kJ/mol\right)$

H_i : Specific mass enthalpy of material stream i $\left(kJ/kg\right)$

$\dot{m}_i$: Mass flow rate of material stream i $\left(kg/s\right)$

M_j : Molecular weight of the j-th species $\left(kg\ j/mol\right)$

$\dot{n}_i$: Molar flow rate of material stream i $\left(mol/s\right)$

P_0 : Reference pressure $\left(bar\right)$

$\dot{Q}_j$: Rate of heat entering the system at temperature $T_{\sigma,j}$ $\left(kW\right)$

$\dot{Q}_{real}$: Rate of heat entering/leaving the hydrogen combustion system at temperature T_{surr} $\left(kW\right)$

s_i : Specific molar entropy of material stream i $\left(kJ/mol\,K\right)$

S_i : Specific mass entropy of material stream i $\left(kJ/kg\,K\right)$

$\dot{S}_{gen}$: Rate of entropy generation in hydrogen combustion subsystem $\left(kJ/K/s\right)$

S_C : Index set of components (species) present in at least one material stream

S_E : Index set of constituent elements

$\dot{S}_G$: Rate of entropy generation $\left(kJ/K/s\right)$

S_I : Index set of inlet material streams

S_O : Index set of outlet material streams

S_w : Index set of work rates entering (consumed by) and exiting (produced by) the system

T_0 : Reference temperature $\left(K\right)$

T_{surr} : Reference temperature of surrounding for the hydrogen combustion subsystem $\left(K\right)$

$T_{\sigma,j}$: Temperature at $_{\sigma,\,j}$ surroundings region $\left(K\right)$

$\dot{W}_{s,j}$: Rate of shaft work consumed by the *j*-th source in the system $\left(kW\right)$

$\dot{W}_s$: Rate of shaft work entering (consumed by) the system $\left(kW\right)$

$\dot{W}_{real}$: Rate of shaft work entering/leaving the hydrogen combustion system $\left(kW\right)$

$x_{i,j}$: Mass fraction of *j*-th species in stream i $\left(kg\ j/kg\right)$

X : Oxygen to acetic acid molar ratio

Y : Hydrogen to acetic acid molar ratio for case 2

Greek Letters:

$\Delta g_{f,i}^{0}$: Standard state Gibbs free energy of formation of the *i*-th species $\left(kJ/mol\right)$

$\Delta\dot{G}_s$: Rate of Gibbs free energy change of system $\left(kJ/s\right)$

$\Delta h^0_{f,i}$: Standard state enthalpy of formation of the *i*-th species $\left(kJ/mol\right)$

Δh^0_r : Standard state enthalpy of reaction $\left(kJ/mol\right)$

$\Delta\dot{H}_s$: Rate of enthalpy change of system $\left(kJ/s\right)$

$\Delta s^0_{f,i}$: Standard state entropy of formation of the *i*-th species $\left(kJ/mol\,K\right)$

$\nu_{j,k}$: Stoichiometric coefficient of element k in the *j*-th species

Ω : Open, well delimited system or control volume

η : Efficiency of hydrogen combustion subsystem

ACKNOWLEDGEMENT

I am grateful to God for the grace to start and finish this research work. I am also thankful to my advisor, Prof. Vasilios Manousiouthakis, for the wisdom and grace applied in shaping the way I think. I also acknowledge the support of Patricia Pichardo whose efforts helped in no small way in getting this task done. This work is intended for publication in a research journal with Vasilios Manousiouthakis as the corresponding author.

1. INTRODUCTION

Acetic acid is used as a chemical intermediate in the production of other useful chemicals, such as vinyl acetate, whose derivatives are raw materials for the manufacture of adhesives, coatings, textile finishes, cement additives, packaging film and laminated safety glass for automotive and architectural applications. Acetic acid is also used to manufacture acetic anhydride and cellulose acetate, which are also raw materials in the production of coatings, cellulose plastics, aspirin, acetaminophen, cigarette filter tows and filament yarn. Finally, acetic acid is also a process solvent used in the production of purified terephthalic acid (PTA) from which polyester (PET) fiber, film and resin are made [1, 2, 3]. Because of its wide range of applications, the global demand of acetic acid was valued at 12.1 million metric tons in 2014 and it is expected to reach 16.2 million metric tons per year by 2020 with a compound annual growth rate (CAGR) of 4.9% [4]. The global market is also expected to reach USD 12.2 billion per year by 2020 [5].

Acetic acid has been produced in a wide variety of ways through biological and chemical processes. The biological production of acetic acid involves the traditional and historical "two-step vinegar" process; the first step involves the breakdown of glucose to ethanol and carbon dioxide, while the second step involves the oxidation of ethanol to acetic acid and water. The first step is accomplished using an anaerobic yeast, such as *Saccharomyces cerevisiae* at 300 K with yield of about 90%, while the second step is facilitated by aerobic bacteria, typically *Acetobacter aceti* at 300 – 310 K with a yield of about 85% [1]. The chemical production of acetic acid includes processes such as hydrocarbon oxidation, synthesis gas based synthesis routes, and alcohol carbonylation. A brief description of the various chemical processes employed in the production of acetic acid is provided next.

One of the older acetic acid production methods involves hydrocarbon oxidation. Vapor phase oxidation of ethylene first yields acetaldehyde (Wacker Process), and subsequently further oxidation, in the presence of manganese acetate catalyst, yields acetic acid; this process occurs at pressure ranges of 3 – 10 bar and temperature ranges of 60 – 80°C. This route was plagued by high feedstock costs and a very corrosive catalyst system. Therefore, despite the high yields of acetic acid (90%) and relatively low capital cost, many plants operating with this technology have been shut down over the last 20 years [1, 2, 3]. Other olefins that have been explored as feedstocks include propylene, butenes, and higher olefins, but these processes have not been commercialized because of unfavorable economics [1]. The direct oxidation of saturated hydrocarbons, such as ethane, propane, butane and higher paraffins, to acetic acid has also been reported in the literature (patent and otherwise) [1, 2, 3]. Among these works, the liquid phase oxidation of butane has received the most attention, as commercial plants utilizing this process have become operational. This process yields a myriad of by-products such as methyl ethyl ketone, ethyl acetate, methyl vinyl ketone, formic acid, and propionic acid, depending on reaction conditions and catalyst choice [1].

Synthesis gas is commonly derived from coal, oil, and natural gas resources. Synthesis gas routes to acetic acid include dimethyl ether (DME) carbonylation and methyl formate isomerization, with both DME and methyl formate generated from syngas feedstock. Acetic acid is also produced via methane carbonylation, where the positive change in Gibbs free energy condition of this reaction is overcome by high pressure or strong acid conditions. This process suffers from low yields of acetic acid, low conversion of methane and it produces copious amounts of by-products [3]. Acetic acid has also been reported to be produced directly from methane and carbon dioxide in the presence of oxygen over a vanadium-palladium-aluminum oxide catalyst [6]. The carbonylation

of alcohols is the current state-of-the-art (SOTA) acetic acid commercial production route. One of the main technologies in this space is BP's CATIVA process, which carries out methanol carbonylation using an Iridium based catalyst with an iodide as catalyst promoter. In this process, methanol and carbon monoxide are converted to acetic acid over a homogeneous iridium-based catalyst system. The iridium-based CATIVA process offers significant advantages over the earlier but similar rhodium-based Monsanto process, as it boasts reduced water levels, reduced by-product formation, low organic iodide impurities and low cost [2, 7, 8, 9, 10].

Hydrogen, like acetic acid, has a lot of uses. It is used to produce ammonia for the fertilizer industry, in the refining industry for hydrocracking and hydroprocessing, as fuel for propellants in the aerospace industry and for power generation in fuel cells for automotive and stationary applications. Hydrogen, when used as fuel, produces no greenhouse gas or environmental pollutants such as carbon dioxide, soot or particulates. It also boasts higher power generation efficiencies than most fossil fuels, when used in fuel cell and turbine combustion applications. It is also used for the hydrogenation of fats, as a reducing agent in iron metallurgy and in metal processing. When combined with carbon monoxide as syngas, it finds even more uses in the chemical industry. These include but are not limited to methanol and higher alcohol synthesis, hydrocarbon synthesis via the Fisher-Tropsch process, formic acid and acetic acid synthesis, glycol synthesis and aldehyde formation via hydroformylation [11]. Industrially, hydrogen is produced mostly from natural gas, oil and coal through steam methane reforming (SMR), hydroprocessing (in crude oil refining) and gasification respectively.

As discussed above, natural gas is used as raw material for both acetic acid, and hydrogen production. It is a readily available low-cost commodity, whose 2016 annual U.S. production was 2.239 trillion cubic feet [12]. Processes converting natural gas to chemicals (such as acetic acid

and hydrogen) or to power, generate carbon dioxide emissions, whose geological sequestration has given rise to carbon capture systems. These typically involve carbon dioxide adsorption in solid sorbents, or absorption in liquids (often amine-based). A review of such capture technologies, in the context of hydrogen production from coal/oil/natural gas, can be found in [13].

In this work, the primary motivation for the co-production of hydrogen with acetic acid is to demonstrate the technical feasibility, using currently available technologies, and subsequently the financial benefits, of transforming a carbon and hydrogen containing feedstock, such as natural gas (methane), into hydrogen, without generating carbon dioxide emissions. Indeed, it is shown that the redirection of all the carbon contained in the natural gas into a saleable chemical like acetic acid, is possible by interconnecting in a novel manner currently available technologies, and economically desirable, as it improves the economics of hydrogen production. In the past, a process has been described producing acetic acid via partial oxidation of methane and methanol carbonylation, with the products of the partial oxidation reactor fed directly into the methanol carbonylation reactor. Nevertheless, this process generates carbon dioxide as a byproduct [14]. The work put forward here differs from this earlier work in that it not only sets forth a process to produce acetic acid from natural gas, but does so by co-producing hydrogen and simultaneously eliminating carbon dioxide emissions. The proposed process involves the novel integration of hydrogen and acetic acid production in a modular, cost effective and environmentally friendly manner, and is based entirely on well-known, commercially available technologies.

This work and associated conceptual methodology builds on research presented in [15], that focuses on the co-production of hydrogen with a valuable carbon-containing chemical, formic acid, from natural gas. This work explores another valuable carbon-containing chemical, acetic acid, alongside the co-production of hydrogen. Two case scenarios are explored: the co-production

of acetic acid and hydrogen, and the co-production of acetic acid and power. The two cases are inter-related, as the hydrogen generated in the first case is considered to be readily converted to power in the second case, using either a hydrogen combustion turbine or a hydrogen fuel cell.

The remainder of the manuscript is structured in the following format: First, an overall reaction for the considered process is proposed, and a thermodynamic analysis is carried out to identify thermodynamic limitations imposed on the system to achieve energetic self-sufficiency, as defined in [15], for an open system. Next, a reaction scheme (cluster) whose sum results in the proposed overall reaction is determined. Having established the necessary and sufficient conditions for energetic self-sufficiency, a flowsheet is developed that accomplishes the desired result of co-production of acetic acid and hydrogen. Following the generation of a successful flowsheet, a detailed heat and power integration is carried out on the flowsheet to determine an exact value of a defined intrinsic variable (ratio of oxygen feed to acetic acid) corresponding to an energetic self-sufficient process. A preliminary economic analysis, and a carbon dioxide cost and performance metric calculation as defined in [16], is then performed on the proposed product(s) and system to quantify the profitability and carbon capture potential of the overall process.

2. THERMODYNAMIC AND ENERGETIC SELF SUFFICIENCY CONSTRAINTS ON PROPOSED SYSTEM

The constraints on the system are defined in the context of thermodynamics and energetic self-sufficiency. The overall reaction for the conversion of natural gas (methane) to acetic (ethanoic) acid, and hydrogen, with oxygen as a co-feed, and water as either a co-feed or a co-product, is:

$$2CH_4 + X\,O_2 + 2(1-X)\,H_2O \rightarrow CH_3COOH + 2(2-X)\,H_2 \qquad (R1)$$

where X is the molar flow ratio of oxygen to acetic acid. From the stoichiometry of (R1), it is trivial to establish the following equivalent relations: for hydrogen production, $X \leq 2$; for oxygen consumption, $X \geq 0$; and for water production, $X > 1$. Therefore, a necessary and sufficient condition for hydrogen production and oxygen consumption is $0 \leq X \leq 2$. We now briefly review the concept of energetic self-sufficiency for an open system as defined in [15].

Definition: Let Ω be a steady-state open system with inlets in S_I, outlets in S_O, no heat transferred from the surroundings to the system, heat possibly transferred from the system to the surroundings $\dot{Q}_0 \leq 0$, at the uniform surroundings temperature T_0, and the system's net shaft work to be non-positive $\sum_{j \in S_W} \dot{W}_{s,j} \leq 0$. Such a system is called energetically self-sufficient. Mathematically, it is stated as:

$$\left\{\begin{array}{l}\sum_{i\in S_I}\dot{m}_i-\sum_{i\in S_O}\dot{m}_i=0\\ \sum_{i\in S_I}\sum_{j\in S_C}v_{j,k}\frac{x_{i,j}}{M_j}\dot{m}_i-\sum_{i\in S_O}\sum_{j\in S_C}v_{j,k}\frac{x_{i,j}}{M_j}\dot{m}_i=0 \quad \forall k\in S_E\\ \dot{Q}_0=T_0\cdot\left(\sum_{i\in S_O}S_i\dot{m}_i-\sum_{i\in S_I}S_i\dot{m}_i\right)-T_0\cdot\dot{S}_G\le 0,\ \dot{S}_G\ge 0\\ \sum_{j\in S_W}\dot{W}_{s,j}=T_0\cdot\dot{S}_G-\left(\sum_{i\in S_I}\left(H_i-T_0\cdot S_i\right)\dot{m}_i-\sum_{i\in S_O}\left(H_i-T_0\cdot S_i\right)\dot{m}_i\right)\le 0\end{array}\right\} \quad (1)$$

where S_C and S_E are the sets of all chemical species and chemical elements respectively comprising the system, $v_{j,k}$ is the stoichiometric coefficient of the constituent element k in the formation reaction of the j-th chemical species, $x_{i,j}$ is the mass fraction of the j-th chemical species in the i-th stream, H_i ,and S_i are the specific mass enthalpy, and entropy respectively of the i-th stream at its temperature and pressure conditions T_i and P_i; and $\dot{S}_G$ is the total rate of entropy generation due to irreversibilities both within the system's control volume and in the heat transfer across temperature differences between the control volume and its surroundings [15]. If $T_i=T_0 \ \ \forall i\in S_I\cup S_O$, then $H_i-T_0\cdot S_i=G_i \ \ \forall i\in S_I\cup S_O$, where G_i is the specific Gibbs free energy at the temperature and pressure conditions T_0 and $P_i \ \ \forall i\in S_I\cup S_O$. From eqn. (1), a necessary condition for energetic self-sufficiency is:

$$\left\{\begin{array}{l}\sum_{i\in S_I}H_i\dot{m}_i-\sum_{i\in S_O}H_i\dot{m}_i\ge 0\\ \sum_{i\in S_I}\left(H_i-T_0\cdot S_i\right)\dot{m}_i-\sum_{i\in S_O}\left(H_i-T_0\cdot S_i\right)\dot{m}_i\ge 0\end{array}\right\} \quad (2)$$

Considering that $\{T_i = T_0 = 298\,K \wedge P_i = P_0 = 1\,bar\}\ \ \forall i \in S_I \cup S_O$, the above necessary condition becomes:

$$\left\{\begin{array}{l} \Delta\dot{H}_s\left(T_0, P_0\right) \triangleq \sum_{i\in S_I} H_i\dot{m}_i - \sum_{i\in S_O} H_i\dot{m}_i \geq 0 \\ \Delta\dot{G}_s\left(T_0, P_0\right) \triangleq \sum_{i\in S_I} G_i\dot{m}_i - \sum_{i\in S_O} G_i\dot{m}_i = \sum_{i\in S_I}\left(H_i - T_0\cdot S_i\right)\dot{m}_i - \sum_{i\in S_O}\left(H_i - T_0\cdot S_i\right)\dot{m}_i \geq 0 \end{array}\right\} \quad (3)$$

To further quantify the aforementioned energetic self-sufficiency conditions (both the necessary ones and the necessary and sufficient ones), two approaches are pursued for the evaluation of all required thermodynamic information. The first employs standard state properties and ideal gas and mixture assumptions, while the second employs an equation of state for the mixture, as employed in a commercial simulator like UNISIM™.

Table 1 lists the standard state molar enthalpy, Gibbs molar free energy and molar entropy values for all species [17, 18], and the molar enthalpy, Gibbs molar free energy and molar entropy values from UNISIM, using the Peng-Robinson (PR) equation of state for all species except for acetic acid whose values are calculated using the UNIFAC VLE liquid activity model. By substituting these values into equations (1) and (3), the aforementioned energetic self-sufficiency constraints are determined for two case scenarios: the co-production of acetic acid and hydrogen, (case 1), and the co-production of acetic acid, hydrogen, and power (case 2).

The schematic for case 1 is shown in figure 1, while the schematic for case 2 is shown in figure 2. For case 1, and for a CH_4 inlet molar flow rate of 2 mol/s, the energetic self-sufficiency constraints are summarized in the sets of equations and inequalities presented in (4) (for the standard state) and (5) (for the equation of state) respectively. The first three constraints ensure oxygen consumption, hydrogen production, and nonnegative entropy generation respectively. The fourth

constraint ensures that the enthalpy necessary condition (3) is satisfied, while the fifth and sixth constraints ensure heat removal and work generation respectively.

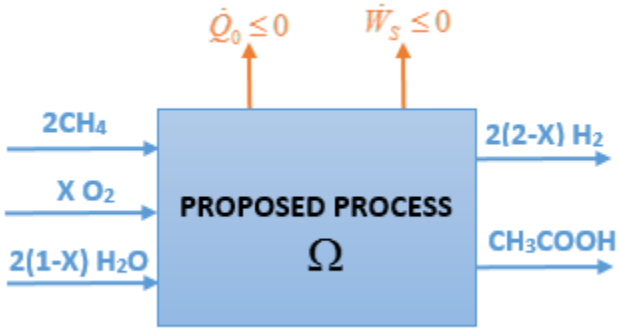

Figure 1: Schematic of process for co-production of acetic acid and hydrogen from natural gas

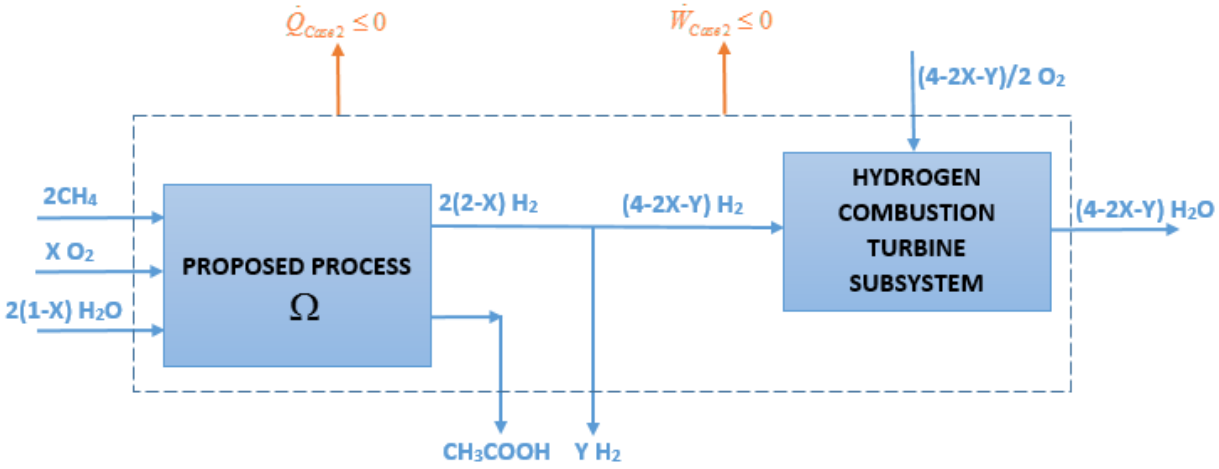

Figure 2: Schematic of process for co-production of acetic acid and power from natural gas

Table 1: Molar enthalpies, Gibbs free energies and entropies of formation of various chemical species at 1 bar, 298 K.

Species	Standard state values $\Delta h^0_{f,i}$ (kJ/mol)	UNISIM h_i (kJ/mol)	Standard state values s^0_i (kJ/mol K)	UNISIM s_i (kJ/mol K)	Standard state values $\Delta g^0_{f,i}$ (kJ/mol)	UNISIM g_i (kJ/mol)

CH_4 (g)	-74.520	-74.92	0.186	0.184	-50.460	-129.63
H_2O (l)	-285.830	-286.20	0.070	0.054	-237.129	-302.20
CH_3COOH (l)	-484.500	-460.60	0.160	0.071	-389.900	-481.76
CO (g)	-110.525	-110.60	0.198	0.159	-137.169	-157.98
CO_2 (g)	-393.509	-393.80	0.214	0.173	-394.359	-445.35
H_2 (g)	0	-0.0044	0.131	0.123	-	-36.66
O_2 (g)	0	-0.0138	0.205	0.1451	-	-43.25

$$\left\{\begin{array}{l} 0 \le X \le 2,\ \dot{S}_G \ge 0 \\ X \ge 0.413 \\ X \ge -3.062\,\dot{S}_G + 0.52 \\ X \ge 0.628\,\dot{S}_G + 0.391 \end{array}\right\} \qquad (4)$$

$$\left\{\begin{array}{l} 0 \le X \le 2,\ \dot{S}_G \ge 0 \\ X \ge 0.457 \\ X \ge -3.532\,\dot{S}_G + 0.307 \\ X \ge 0.611\,\dot{S}_G + 0.482 \end{array}\right\} \qquad (5)$$

Comparison of (4) and (5) above indicates a minimal deviation from ideality. Nevertheless, the equation of state based constraints (5) are employed in figure 3 below, to identify the energetic self-sufficiency feasible region in $X - \dot{S}_G$ space, for case 1. As shown in figure 3, the heat removal constraint, $X \ge -3.532\,\dot{S}_G + 0.307$, is irrelevant to the determination of the energetic self-sufficiency feasible region in $X - \dot{S}_G$ space.

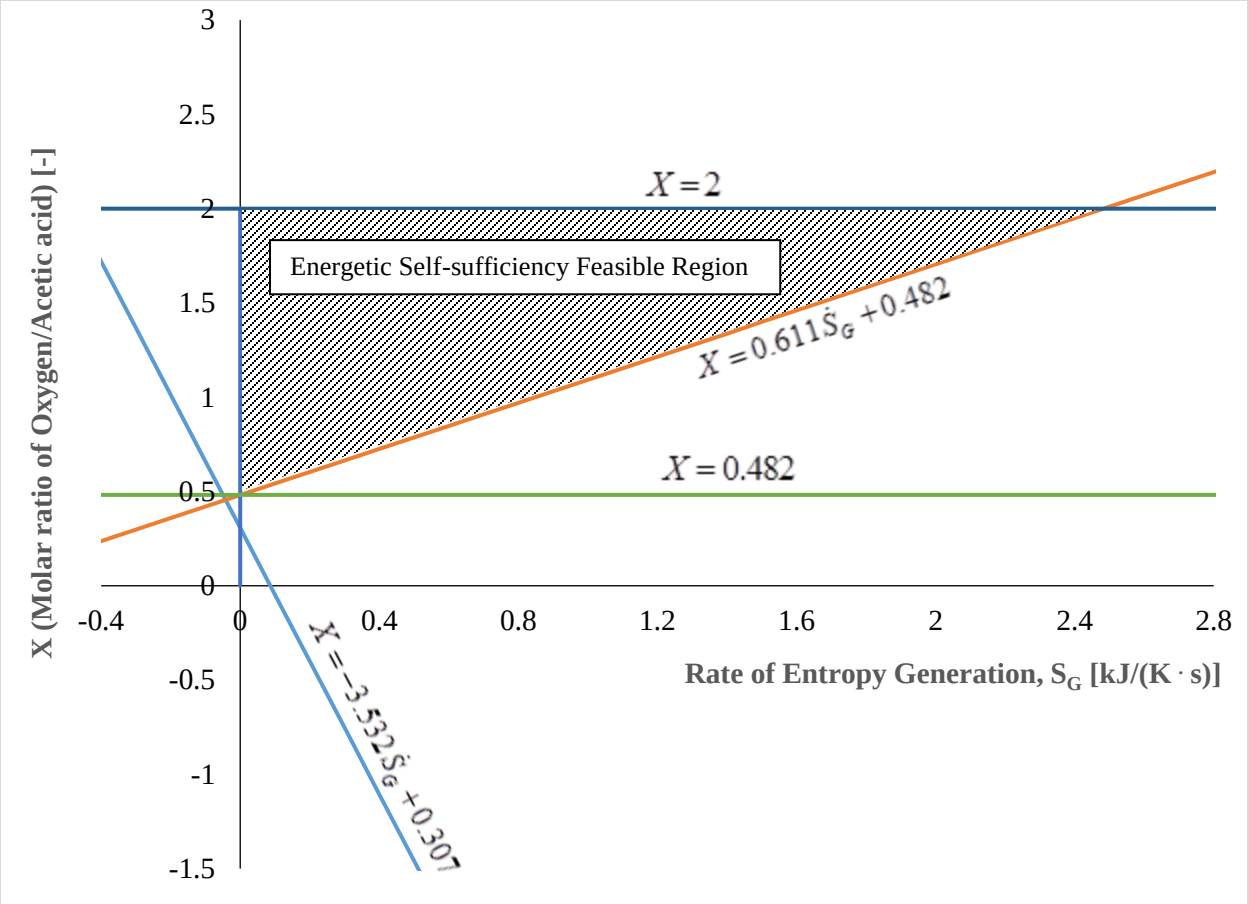

Figure 3: Energetic self-sufficiency feasible region in (X, S_G) space for Case 1

The above analysis is repeated for case 2 which employs the following two reaction cluster:

$$2CH_4 + X\,O_2 + 2(1-X)\,H_2O \rightarrow CH_3COOH + 2(2-X)\,H_2 \qquad (R1)$$

$$(4-2X-Y)\,H_2 + (2-X-\frac{Y}{2})O_2 \rightarrow (4-2X-Y)\,H_2O \qquad (R2)$$

$$2CH_4 + \left(2-\frac{Y}{2}\right)O_2 + (Y-2)\,H_2O \rightarrow CH_3COOH + Y\,H_2 \qquad (R3)$$

For case 2, and for a CH_4 inlet molar flow rate of 2 mol/s, the energetic self-sufficiency constraints are summarized in the sets of equations and inequalities presented in (6) (for the standard state) and (7) (for the equation of state) respectively. The first two constraints ensure oxygen

consumption, and hydrogen production for subsystem Ω. The third constraint ensures nonnegative entropy generation for the whole system. The fourth constraint ensures heat removal from subsystem Ω, while the fifth constraint ensures hydrogen consumption as well as heat and work removal from the ideal hydrogen combustion turbine subsystem. The sixth constraint ensures work generation from the overall system. The seventh and last constraint ensures that hydrogen production is nonnegative.

$$\left\{\begin{array}{l} 0 \le X \le 2,\ \dot{S}_G \ge 0 \\ X \ge -3.062\,\dot{S}_G + 0.52 \\ X \le -0.5Y + 2 \\ X \le -8.19\dot{S}_G - 7.02Y + 22.98 \\ Y \ge 0 \end{array}\right\} \tag{6}$$

$$\left\{\begin{array}{l} 0 \le X \le 2,\ \dot{S}_G \ge 0 \\ X \ge -3.532\,\dot{S}_G + 0.307 \\ X \le -0.5Y + 2 \\ X \le -13.06\dot{S}_G - 11.19Y + 34.46 \\ Y \ge 0 \end{array}\right\} \tag{7}$$

The equation of state based constraints (7) are employed in figure 4 below to identify the energetic self-sufficiency feasible region in $X - \dot{S}_G$ space for case 2. As shown in figure 4, one boundary of the feasible region is dependent on Y and case 2 reduces to case 1 when $Y = 2(2 - X)$.

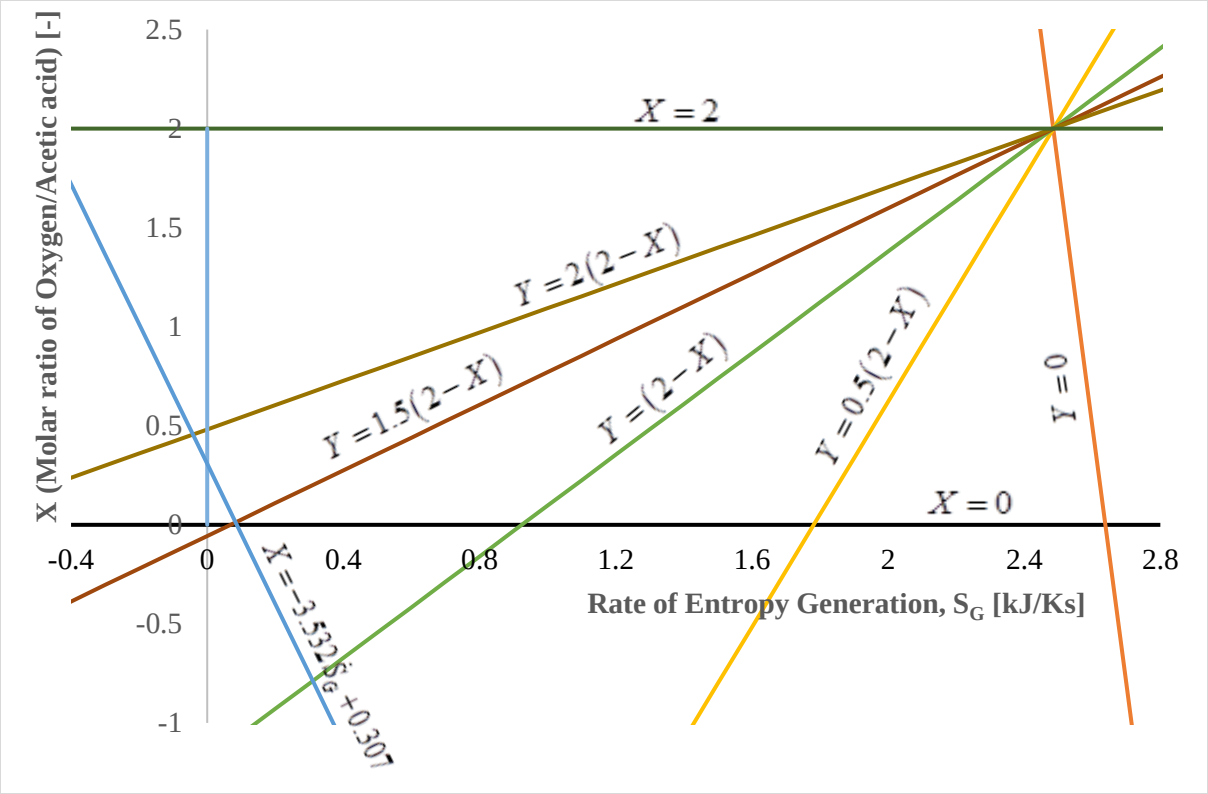

Figure 4: Energetic self-sufficiency feasible region in (X, S_G) space for case 2.

3. REALIZATION OF PROPOSED ACETIC ACID AND HYDROGEN CO-PRODUCTION PROCESS

As stated earlier, in this work a novel chemical process is developed that actualizes reaction (R1), also shown below. Since no single step process exists for the realization of (R1), its realization is sought through the creation of a reaction cluster [19, 20, 21, 22], also frequently referred to as a Solvay cluster, whose overall reaction (i.e. the stoichiometric sum of all cluster reactions) is the desired reaction (R1). Such a novel reaction cluster is proposed below. The cluster reactions are shown in Figure 5.

$$\left(\frac{2X}{3}\right)\left[CH_4^{(g)} + 1.5O_2^{(g)} \rightarrow CO^{(g)} + 2H_2O^{(g)}\right] \quad (R4)$$

$$\left(1-\frac{X}{3}\right)\left[CH_4^{(g)} + H_2O^{(g)} \rightleftharpoons CO^{(g)} + 3H_2^{(g)}\right] \quad (R5)$$

$$\left(1-\frac{X}{3}\right)\left[CH_4^{(g)} + 2H_2O^{(g)} \rightleftharpoons CO_2^{(g)} + 4H_2^{(g)}\right] \quad (R6)$$

$$\left(1-\frac{X}{3}\right)\left[CO_2^{(g)} + H_2^{(g)} \rightleftharpoons CO^{(g)} + H_2O^{(g)}\right] \quad (R7)$$

$$CO^{(g)} + 2H_2^{(g)} \rightarrow CH_3OH^{(g)} \quad (R8)$$

$$CO^{(g)} + CH_3OH^{(g)} \rightarrow CH_3COOH^{(l)} \quad (R9)$$

$$2CH_4^{(g)} + X\,O_2^{(g)} + 2(1-X)H_2O^{(g)} \rightleftharpoons CH_3COOH^{(l)} + 2(2-X)H_2^{(g)} \quad (R1)$$

Figure 5: Reaction cluster generating acetic acid and hydrogen from natural gas

The reaction cluster consists of the incomplete combustion of methane (R4), Steam Methane Reforming (SMR), (R5) and (R6), Reverse Water Gas Shift reaction (RWGS), (R7), methanol synthesis from syngas, (R8), and acetic acid synthesis through methanol carbonylation, (R9).

The above described reaction cluster leads to the conceptual design of a process that realizes the overall reaction (R1), while utilizing well established technologies. The resulting process can be organized into six subsystems that are described below:

3.1 Incomplete Combustion (IC) of Methane Subsystem

The Incomplete Combustion subsystem is shown in Figure 6. Pure oxygen is mixed with a fresh methane feed and the mixture is brought to the operating conditions of the combustion reactor at 1 bar, 1273 K. The supply of oxygen is controlled such that the only products of combustion are carbon monoxide, CO, and water, H_2O. The gaseous product from the incomplete combustion reactor is cooled to 311 K and flashed to remove water. The high purity CO is then compressed to 26.9 bar and mixed with CO exiting the carbon dioxide adsorption unit. The incomplete combustion of methane serves not only as a CO generator, but also as an energy source for the highly endothermic steam methane reforming (SMR) subsystem, which is described next.

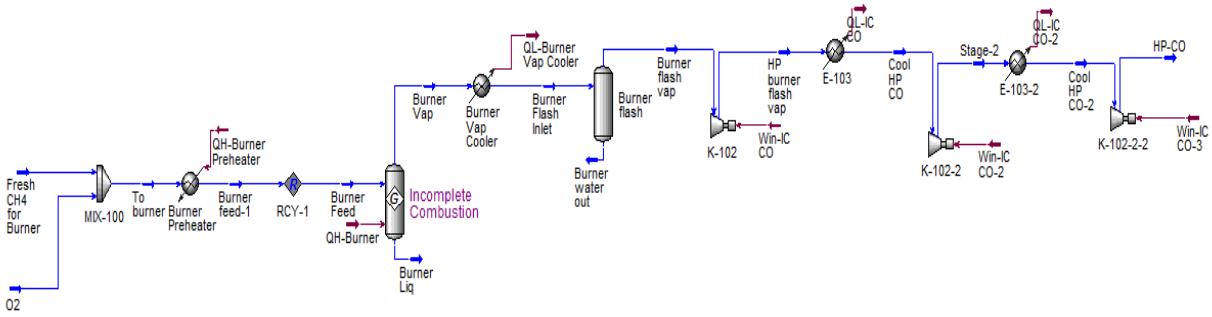

Figure 6: Incomplete Combustion (IC) subsystem.

3.2 Steam Methane Reforming (SMR) Subsystem

Fresh methane feed and water are fed into this subsystem at atmospheric conditions and brought up to a pressure of 26.9 bar (using compressor and pumping operations respectively), and

subsequently to a temperature of 1262 K, values which are consistent with typical SMR operating conditions (15 – 30 bar, 900 K – 1273 K) [13, 23, 24]. The SMR feed consists of excess steam, generated from recycled water. The feed to the reactor consists of a steam/methane ratio of 3.5. The excess steam in the SMR reactor feed serves to reduce carbon formation [15, 25, 26, 27] and ensures a high conversion of methane. At these operating conditions, the conversion of methane is about 99% and the SMR product consists of hydrogen, steam, carbon monoxide and carbon dioxide. The product is cooled to 311 K, flashed to remove water, and sent to a hydrogen membrane separator to separate hydrogen. The behavior of the SMR unit can be captured by considering that two reforming reactions take place ((R5), (R6) shown below).

$$CH_4 + H_2O \rightleftharpoons CO + 3H_2 \qquad (R5)$$
$$CH_4 + 2H_2O \rightleftharpoons CO_2 + 4H_2 \qquad (R6)$$

The Water Gas Shift (WGS) reaction, ((R10) shown below), is often considered to also take place within the SMR unit.

$$CO + H_2O \rightleftharpoons CO_2 + H_2 \qquad (R10)$$

However, at equilibrium, the WGS reaction is linearly dependent on the two aforementioned reforming reactions, and thus need not be considered. Given that SMR units are typically operated in practice near equilibrium conditions, the SMR unit in this work is modeled using a Gibbs equilibrium reactor, whose outlet consists of CH_4, H_2O, H_2, CO_2 and CO, and can be captured by (R5), and (R6). The SMR subsystem is shown in Figure 7. The SMR product is cooled, flashed to remove water, and sent to the H_2 membrane separator for H_2 separation.

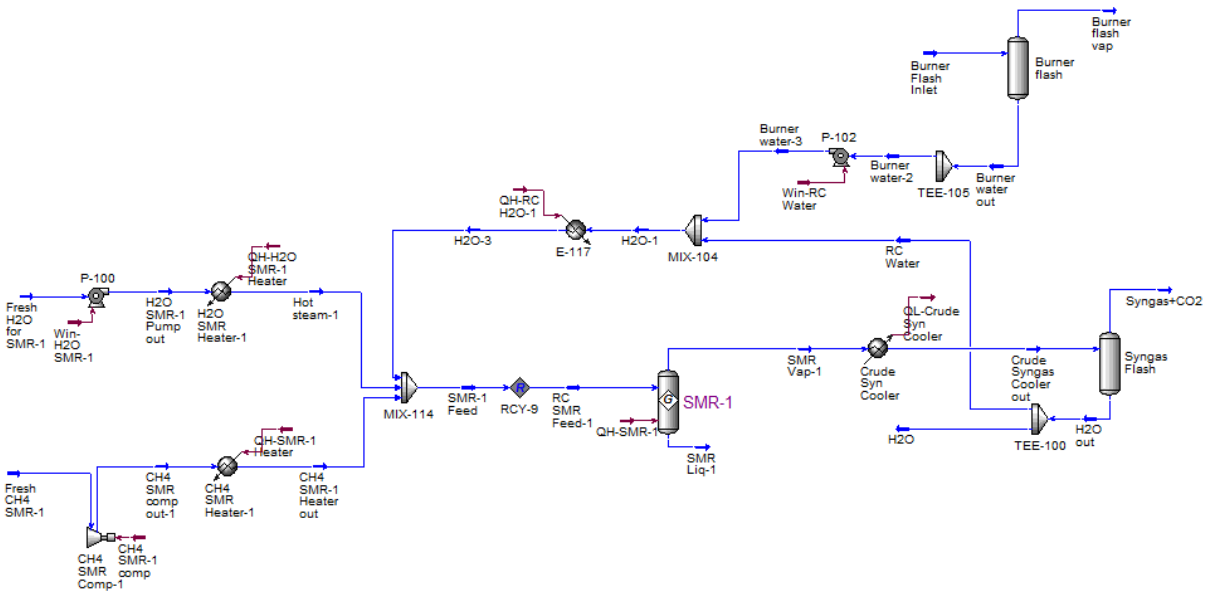

Figure 7: Steam Methane Reforming (SMR) subsystem

3.3 Reverse Water Gas Shift (RWGS) Subsystem

To attain zero carbon dioxide emissions, a means of reducing CO_2 must be incorporated into the overall system. The RWGS reaction, (R7), is utilized to convert CO_2 to CO needed to produce methanol and acetic acid. This subsystem is shown in Figure 8. Pure H_2 at 26.9 bar is used as flush gas to remove CO_2 from the CO_2 adsorption unit (subsystem 4), resulting into an adsorption unit outlet consisting of H_2 and CO_2 at 26.9 bar, 523 K. The mixture is heated to 1173 K [28, 29, 30], and fed to the RWGS reactor. The RWGS forward reaction is limited by the amount of hydrogen available because of the competing demand of hydrogen for sale/power generation and methanol synthesis. From a thermodynamics standpoint, the RWGS reaction is favored at high temperatures. In addition, high temperatures limit methane formation, via the methanation reaction, (R11) or the Sabatier reaction, (R12) respectively. It has been noted that at temperatures above 973 K, no or

very little methane can be formed [28] and above 1173 K, the danger of coke formation is eliminated [29].

$$CO + 3H_2 \rightleftharpoons CH_4 + H_2O \qquad (R11)$$

$$CO_2 + 4H_2 \rightleftharpoons CH_4 + 2H_2O \qquad (R12)$$

The gaseous product of the RWGS reactor is cooled to 311 K, flashed to remove water, and mixed with the hydrogen-lean mixture exiting the hydrogen membrane separator unit containing mostly CO and CO_2. The commingled stream is heated to 523 K and fed to the CO_2 adsorption unit for CO_2 separation.

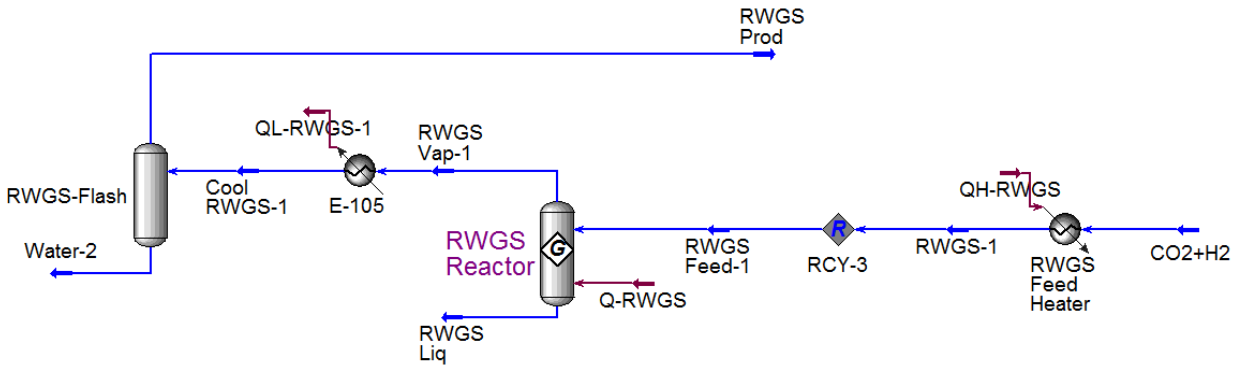

Figure 8: Reverse Water Gas Shift (RWGS) Subsystem

3.4 Gaseous separation subsystem (H_2 membrane separator and CO_2 Adsorption unit)

The cooled SMR reactor product at 26.9 bar, 311 K after flashing is sent to a hydrogen palladium membrane separator to separate hydrogen [31]. During operation, hydrogen permeates through the palladium membrane and is evacuated with saturated steam at 14 bar. The steam flow rate is adjusted so that an equimolar amount of steam and hydrogen exits the membrane separator. The

steam-hydrogen permeate is cooled to 311 K and flashed to remove and recycle water yielding a 99% pure hydrogen stream. The hydrogen membrane separator is modelled as a 95% efficient component splitter with two exit streams: a steam-hydrogen mixture leaving at 14 bar, 470 K and a mixture of CO, CO_2 and small amounts of H_2 leaving at 26.9 bar, 311 K. The highly pure hydrogen stream is split to serve as feed for the methanol synthesis subsystem and the RWGS reactor subsystem, while excess hydrogen is made available either as a saleable product (at atmospheric conditions) or as fuel for power generation in a hydrogen combustion turbine subsystem.

The H_2-lean retentate from the hydrogen membrane separator is sent to a CO_2 adsorption unit operated at 26.9 bar and 523 K, and using as adsorbent layered double hydroxides (LDH) (often also referred to as hydrotalcites), a class of anionic and basic clays [32, 33]. CO_2 adsorption forms part of the novel Hybrid Adsorbent Membrane Reactor (HAMR) system outlined in [32] in experiments utilizing the Water Gas Shift (WGS) reaction. This adsorption unit is employed here as it permits the high temperature adsorption of CO_2, thus reducing the amount of heat needed to raise the temperature of the reactants to the reaction temperature of the RWGS reaction. Pure hydrogen is used as sweep gas to remove the adsorbed CO_2 from the LDH, as a H_2, CO_2 mixture is needed as feed for the RWGS reactor. The adsorption process is deemed adiabatic and isothermal with steady-state application. Two streams exit the CO_2 adsorption unit: A CO rich (95%) stream at 26.9 bar and 523 K, and a mixture of H_2 and CO_2 at the same conditions. The CO stream is split to service the methanol synthesis and acetic acid synthesis (methanol carbonylation) reactors, while the H_2 and CO_2 mixture acts as feed for the RWGS reactor. The gaseous separation subsystem is shown in Figure 9.

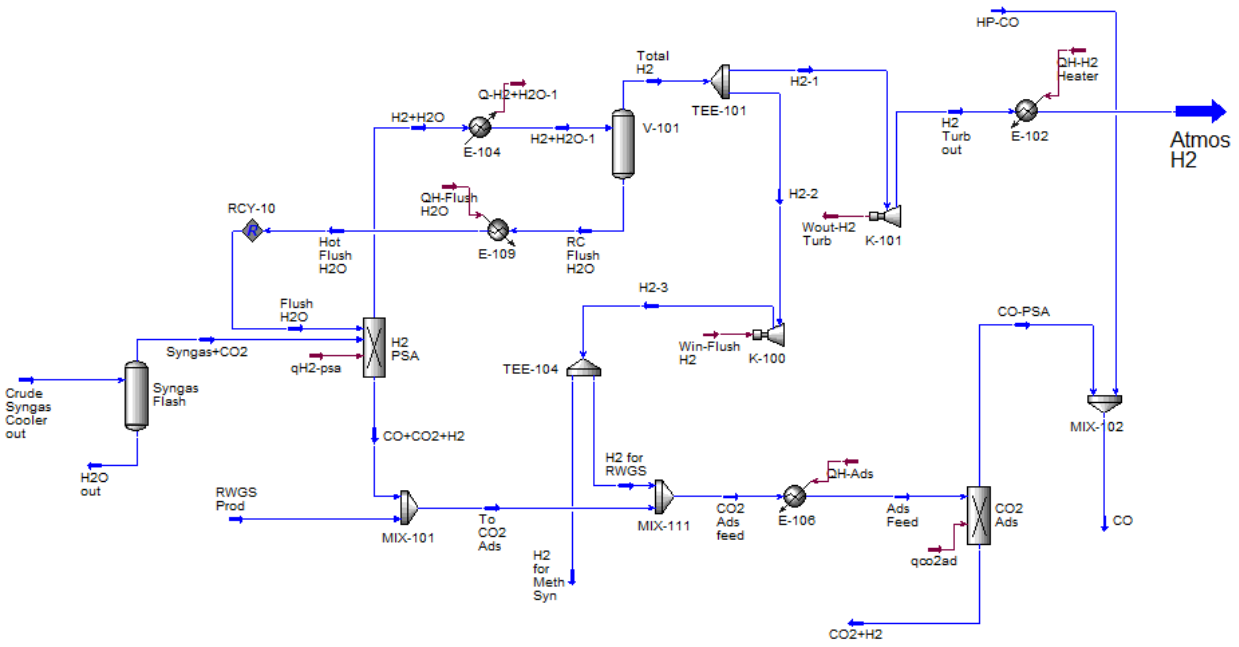

Figure 9: Gaseous Separation Subsystem

3.5 Methanol Synthesis Subsystem

Methanol is produced from H_2 and CO at pressure ranges of 35 bar – 100 bar and temperature ranges of 473 K – 573 K [34, 35, 36, 37, 38]. The methanol subsystem is shown in Figure 10. CO from the CO_2 adsorption unit is mixed with hydrogen from the H_2 membrane separator and the mixture is compressed to the operating pressure, 50 bar, and cooled to the operating temperature, 523 K, of the methanol synthesis reactor. The feed to the methanol synthesis reactor is then constituted by mixing the aforementioned stream with recycled syngas from the methanol synthesis reactor. The syngas is converted to methanol using a $CuO/ZnO/Al_2O_3$ catalyst at a per pass CO conversion of 35% at these operating conditions [39, 40]. It has been noted in literature that CO_2 plays a part in methanol synthesis and as such CO_2 forms part of the feed with typical CO_2 feed concentrations ranging from 3 – 8 mole percent [36, 38, 41, 42]. For model simplicity, however, CO_2 is not included in the methanol reactor feed and methanol is considered generated

only from CO and H_2. This assumption is justified in that we account for more carbon dioxide within the process, in terms of equipment sizing and capital cost, than necessary. Hydrocarbons may also be formed because of the direct hydrogenation of carbon monoxide [42], but this too is not considered in the model. From a practical standpoint, any hydrocarbon formed can be routed to the burner and consumed to produce CO, H_2O and energy. However, increased costs resulting from additional equipment would have to be taken into consideration. Gaseous methanol product is cooled to 308 K to separate methanol from unreacted syngas. The liquid methanol is throttled and reheated to 40 bar, 473 K, to match the operating conditions of the acetic acid synthesis reactor.

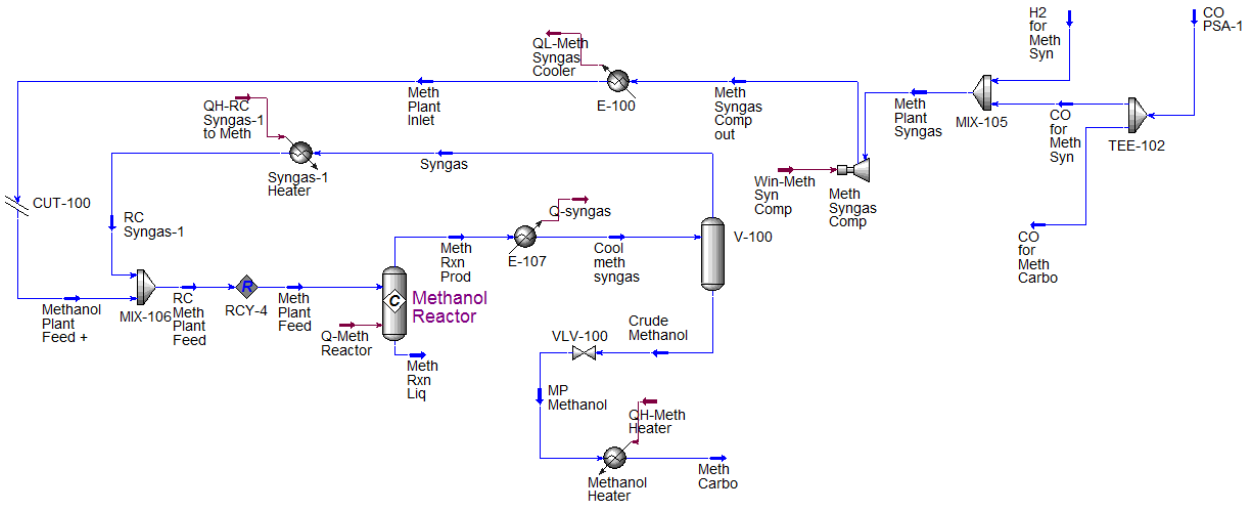

Figure 10: Methanol Synthesis Subsystem

3.6 Acetic Acid Synthesis (Methanol Carbonylation) Subsystem

In this subsystem, acetic acid is produced via methanol carbonylation using the industrial Cativa process which utilizes an iridium catalyst with hydrogen iodide as a promoter (Figure 11). Typical methanol carbonylation reactions are carried out in operating conditions of 30 - 60 bar and 423 K – 493 K [2, 7, 8]. There is an abundance of literature on the reaction mechanism, chemistry and kinetics of the reaction including the reported advantages of this process over the similar but older

BASF and Monsanto processes. The carbonylation process is very complex and forms a host of by-products, primarily propionic acid with varying amounts of methyl iodide, methyl acetate, acetaldehyde and water depending on the reaction conditions and catalyst system in use [3, 9]. One of the proposed mechanisms in which this reaction is thought to occur entails the formation of methyl iodide from methanol, (R13), the carbonylation of methyl iodide to give acetyl iodide, (R14), and the hydrolysis of acetyl iodide to recover HI and yield acetic acid (R15), all in the presence of iridium metal complexes which actively participate to give the overall reaction (R9) [9, 10, 43].

$$CH_3OH + HI \rightarrow CH_3I + H_2O \qquad (R13)$$
$$CH_3I + CO \rightarrow CH_3COI \qquad (R14)$$
$$CH_3COI + H_2O \rightarrow CH_3COOH + HI \qquad (R15)$$
$$\overline{CH_3OH + CO \rightarrow CH_3COOH} \qquad (R9)$$

For model simplicity, only the major reactions involved in the production of acetic acid is considered and as such the simplified reaction scheme of (R13), (R14) and (R15) is utilized. The acetic acid reactor is modeled as a 90% CO conversion reactor with the appropriate reactions specified. The catalyst complexities are thought of as being captured by the hydrogen iodide (HI) component in the model and will be referred to as the catalyst component of the reaction.

Methanol from the methanol synthesis subsystem is mixed with pure CO from the CO_2 adsorption unit at 40 bar, 473 K and fed alongside an iridium/HI catalyst, to the acetic acid synthesis (methanol carbonylation) reactor. Methanol reacts with hydrogen iodide to give methyl iodide and water in equimolar amounts. This mixture reacts with CO to produce acetic acid and HI. At the operating conditions, the reactor liquid effluent comprises of a stream rich in acetic acid with HI and H_2O impurities, while the vapor product consists of a stream rich in HI but lean in acetic acid.

The vapor product stream is recycled to the entrance of the reactor while the liquid product stream is throttled to 6.5 bar and fed to a distillation column for acetic acid separation. The feed to the distillation column is an acetic acid rich stream at 6.5 bar, 424 K. The light end stream recovers 99.9% of the catalyst at 6.5 bar, 306 K. This stream is compressed and cooled to 40 bar, 473 K and recycled to the reactor entrance. The heavy end of the distillation column yields a 96% pure acetic acid at 461 K, which when throttled to 1 bar and cooled to room temperature, exits the flowsheet as a saleable product. A 99.9% purity of acetic acid can be achieved from the distillation column but this is an energy and cost intensive venture.

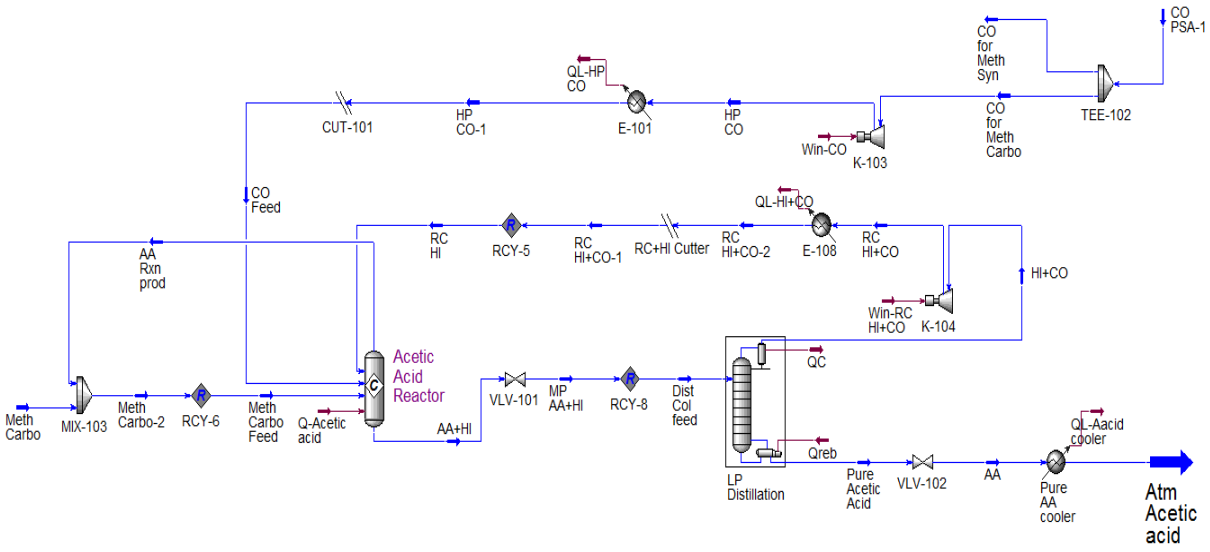

Figure 11: Acetic acid Synthesis Subsystem

4. HYDROGEN COMBUSTION TURBINE SUB-SYSTEM THERMODYNAMIC ANALYSIS

As mentioned earlier, one possible way to generate power from this process, without generating carbon dioxide emissions, is to combust some or even all of the produced hydrogen in a combustion turbine. The generated power is first used to meet the flowsheet's power consumption needs, and the excess power, if any, is made available as commodity to be sold for profit. In this section, the hydrogen's power generation potential is quantified using a thermodynamic analysis of a hydrogen combustion turbine subsystem. A subsystem schematic is shown in Figure 12. It is considered that pure hydrogen and oxygen enter separately the subsystem boundary, and are completely transformed to water according to the combustion reaction (R16):

$$H_2^{(g)} + \frac{1}{2}O_2^{(g)} \rightarrow H_2O^{(g)} \qquad (R16)$$

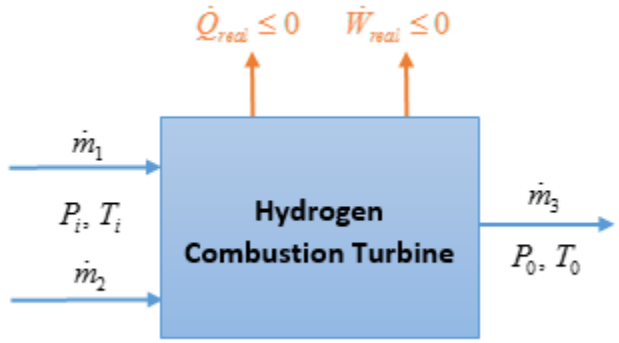

Figure 12: Hydrogen combustion turbine subsystem

The subsystem is considered to operate at steady state, with no accumulation of mass or energy, and to have its outlet at standard conditions, P_0 = 1 bar and T_0 = 298 K, while its inlets depend on the conditions of the hydrogen producing flowsheet considered. The subsystem is energetically

self-sufficient, [15], and is allowed to provide heat (and of course work) to its surroundings. Both an ideal and a real hydrogen combustion turbine subsystem are considered, with identical inlet and outlet characteristics, and the former leading to no entropy generation. The work (power) generation rates of the two aforementioned real and ideal subsystems are related through a combustion turbine subsystem efficiency. Typical values range between 67 - 77% depending on the internal power cycle employed [44]. The resulting thermodynamic model is presented below:

$$\left\{\begin{array}{l} 0=\dot{m}_1+\dot{m}_2-\dot{m}_3 \\ 0=\dot{m}_1H_1+\dot{m}_2H_2-\dot{m}_3H_3+\dot{Q}_{ideal}+\dot{W}_{ideal} \\ 0=\dot{m}_1H_1+\dot{m}_2H_2-\dot{m}_3H_3+\dot{Q}_{real}+\dot{W}_{real} \\ 0=\dot{m}_1S_1+\dot{m}_2S_2-\dot{m}_3S_3+\dfrac{\dot{Q}_{ideal}}{T_{surr}} \\ 0=\dot{m}_1S_1+\dot{m}_2S_2-\dot{m}_3S_3+\dot{S}_{gen}+\dfrac{\dot{Q}_{real}}{T_{surr}} \\ \dot{Q}_{real}\le 0,\ \dot{W}_{real}\le 0,\ \dot{Q}_{ideal}\le 0,\ \dot{W}_{ideal}\le 0,\ \dot{S}_{gen}\ge 0 \end{array}\right\}\Leftrightarrow$$

$$\left\{\begin{array}{l} \dot{m}_3=\dot{m}_1+\dot{m}_2 \\ \dot{W}_{ideal}=\dot{m}_1\left[\left(H_3-T_{surr}S_3\right)-\left(H_1-T_{surr}S_1\right)\right]+\dot{m}_2\left[\left(H_3-T_{surr}S_3\right)-\left(H_2-T_{surr}S_2\right)\right] \\ \dot{W}_{real}=\dot{m}_1\left[\left(H_3-T_{surr}S_3\right)-\left(H_1-T_{surr}S_1\right)\right]+\dot{m}_2\left[\left(H_3-T_{surr}S_3\right)-\left(H_2-T_{surr}S_2\right)\right]+T_{surr}\,\dot{S}_{gen} \\ \dot{Q}_{ideal}=-\dot{m}_1T_{surr}\left(S_1-S_3\right)-\dot{m}_2T_{surr}\left(S_2-S_3\right) \\ \dot{Q}_{real}=-\dot{m}_1T_{surr}\left(S_1-S_3\right)-\dot{m}_2T_{surr}\left(S_2-S_3\right)-T_{surr}\,\dot{S}_{gen} \\ \dot{Q}_{real}\le 0,\ \dot{W}_{real}\le 0,\ \dot{Q}_{ideal}\le 0,\ \dot{W}_{ideal}\le 0,\ \dot{S}_{gen}\ge 0 \end{array}\right\}\Leftrightarrow$$

$$\left\{\begin{array}{l}\dot{m}_3=\dot{m}_1+\dot{m}_2\\ \dot{W}_{ideal}=\dot{m}_1\left[\left(H_3-T_{surr}S_3\right)-\left(H_1-T_{surr}S_1\right)\right]+\dot{m}_2\left[\left(H_3-T_{surr}S_3\right)-\left(H_2-T_{surr}S_2\right)\right]\\ \dot{W}_{real}=\dot{W}_{ideal}+T_{surr}\,\dot{S}_{gen}\\ \dot{Q}_{ideal}=-\dot{m}_1T_{surr}\left(S_1-S_3\right)-\dot{m}_2T_{surr}\left(S_2-S_3\right)\\ \dot{Q}_{real}=\dot{Q}_{ideal}-T_{surr}\,\dot{S}_{gen}\\ \dot{W}_{real}\le 0,\ \dot{Q}_{ideal}\le 0,\ \dot{S}_{gen}\ge 0\end{array}\right\}$$

Defining the efficiency of the hydrogen combustion turbine subsystem as:

$\eta \triangleq \dfrac{\dot{W}_{real}}{\dot{W}_{ideal}}$ then yields:

$$\left\{\begin{array}{l}\dot{m}_3=\dot{m}_1+\dot{m}_2\\ \dot{W}_{ideal}=\dot{m}_1\left[\left(H_3-T_{surr}S_3\right)-\left(H_1-T_{surr}S_1\right)\right]+\dot{m}_2\left[\left(H_3-T_{surr}S_3\right)-\left(H_2-T_{surr}S_2\right)\right]\\ \eta=\dfrac{\dot{W}_{real}}{\dot{W}_{ideal}}=\dfrac{\dot{W}_{ideal}+T_{surr}\,\dot{S}_{gen}}{\dot{W}_{ideal}}=\dfrac{\left[\begin{array}{l}\dot{m}_1\left[\left(H_3-T_{surr}S_3\right)-\left(H_1-T_{surr}S_1\right)\right]+\\ +\dot{m}_2\left[\left(H_3-T_{surr}S_3\right)-\left(H_2-T_{surr}S_2\right)\right]\end{array}\right]+T_{surr}\,\dot{S}_{gen}}{\left[\begin{array}{l}\dot{m}_1\left[\left(H_3-T_{surr}S_3\right)-\left(H_1-T_{surr}S_1\right)\right]+\\ +\dot{m}_2\left[\left(H_3-T_{surr}S_3\right)-\left(H_2-T_{surr}S_2\right)\right]\end{array}\right]}\\ \dot{Q}_{ideal}=-\dot{m}_1T_{surr}\left(S_1-S_3\right)-\dot{m}_2T_{surr}\left(S_2-S_3\right)\\ \dot{Q}_{real}=\dot{Q}_{ideal}-T_{surr}\,\dot{S}_{gen}\\ \dot{W}_{real}\le 0,\ \dot{Q}_{ideal}\le 0,\ \dot{S}_{gen}\ge 0\end{array}\right\} \qquad (8)$$

Hydrogen exits subsystem Ω, and enters the hydrogen turbine combustion subsystem at 14 bar, 311 K. The power generated by the hydrogen combustion subsystem is calculated per unit molar flow rate of hydrogen using the UNISIM values of the appropriate species listed in Table 2. The values are calculated by UNISIM using the Peng-Robinson (PR) Equation of state. An exit

condition of 1 bar, 298 K is imposed on the system. The subscripts 1, 2, 3 denote hydrogen, oxygen and water respectively. The amount of work and heat generated by this ideal subsystem can then be calculated from (8) with the results shown in (9).

Table 2: Specific molar enthalpies and entropies of hydrogen, oxygen and water at 14 bar, 311 K.

	Specific Molar Enthalpy h_i $\left[kJ/mol\right]$	Specific Molar Entropy s_i $\left[kJ/\left(mol\cdot K\right)\right]$
Hydrogen, H_2 (g)	0.3655	0.1023
Oxygen, O_2 (g)	0.2544	0.1241
Water, H_2O (l)	-286.2	0.0537

$$\begin{cases} \dot{W}_{ideal} = -253.74 \quad \left[kW\right] \\ \dot{W}_{real} = -253.74\cdot\eta \ \left[kW\right] \\ \dot{Q}_{ideal} = -32.77 \quad \left[kW\right] \\ \dot{Q}_{real} = -286.51 - \dot{W}_{real} = -286.51 + 253.74\cdot\eta \ \left[kW\right] \end{cases} \tag{9}$$

5. FLOWSHEET SIMULATION OF REACTION CLUSTER REALIZATION

The converged simulation of the complete flowsheet of the proposed process is accomplished by putting together the various subsystems to achieve the production of acetic acid and hydrogen/power with zero net carbon dioxide emissions. The simulation of the proposed flowsheet is carried out using the software UniSim Design R443. The Peng-Robinson Equation of state is used to simulate the Incomplete combustion (IC), Steam Methane Reforming (SMR), and Reverse Water Gas Shift (RWGS) sections of the flowsheet, while for the methanol and acetic acid synthesis sections, the UNIFAC VLE liquid activity model and ideal gas model is used for the liquid and vapor phase respectively [45]. The input streams of the flowsheet consist only of methane, oxygen, and water (as appropriate) at 1 bar, 298 K and the output streams consist of acetic acid, hydrogen and water (as appropriate) at the same conditions. A Gibbs free energy minimization reactor is used to represent the IC, SMR and RWGS reactors, while the methanol and acetic acid synthesis reactors are modeled using a conversion reactor. A schematic of the overall process, which is a combination of the subsystems of Figures 6 – 11, is shown in Figure 13.

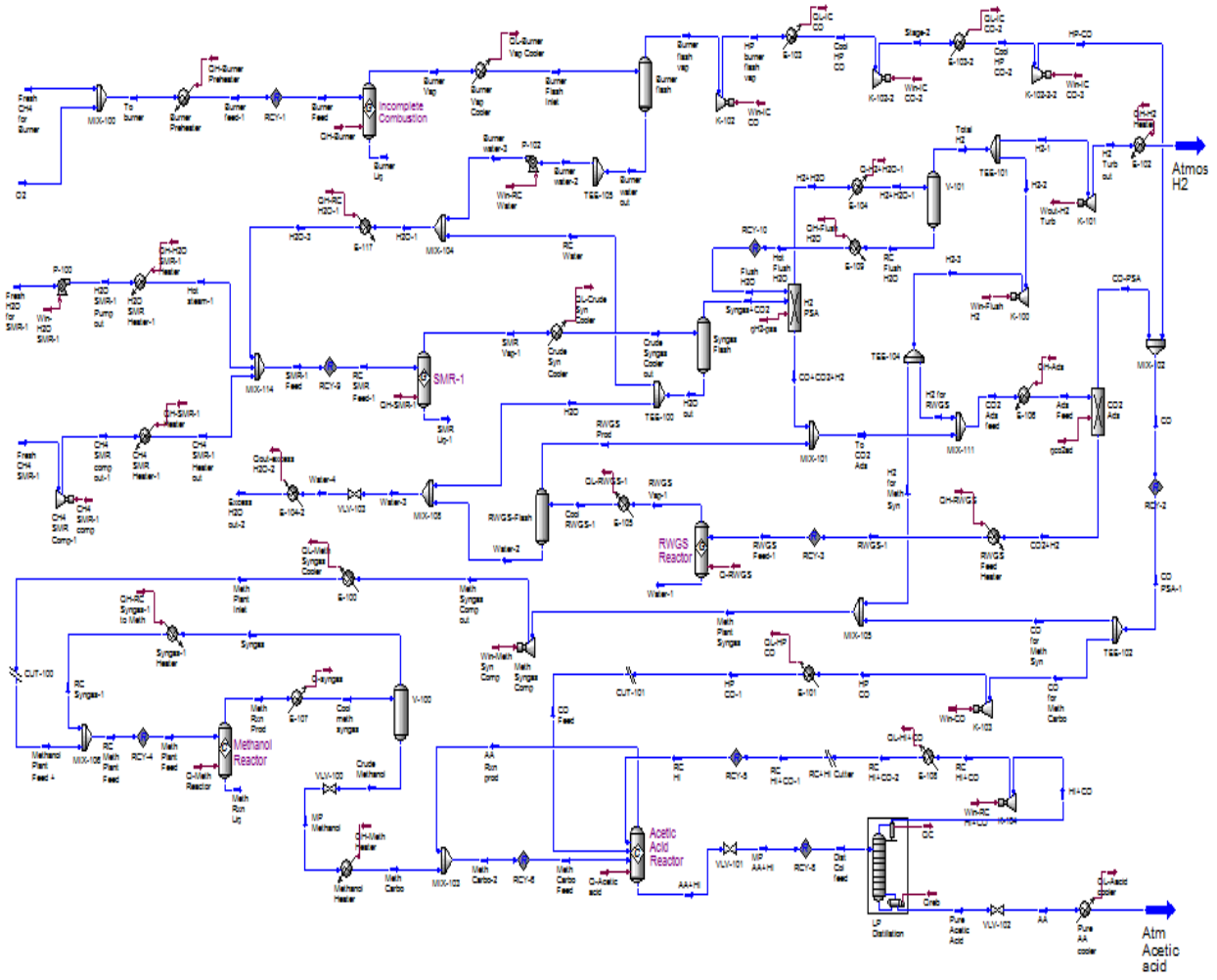

Figure 13: Flowsheet of the Acetic acid and Hydrogen Co-Production Process

The following assumptions are utilized in the development of the process flowsheet:

1. All input feeds to the flowsheet consist of pure components.
2. Pressure losses are neglected in heat exchange devices (heaters and coolers) utilized for heating and cooling operations.
3. All turbine/expanders and pump/compressors are of the centrifugal type with adiabatic efficiencies fixed at 75%.

From a thermodynamics and energetic self-sufficiency point of view, the following inequality must hold for the overall reaction considered: $0.482 \leq X \leq 2$. A value of $X = 0.482$ is used as the initial operating point and the process is repeated for different values of X that satisfy the above inequality.

6. HEAT AND POWER INTEGRATION OF PROPOSED FLOWSHEET FOR THE CO-PRODUCTION OF ACETIC ACID AND HYDROGEN/POWER

The converged flowsheet producing acetic acid and hydrogen/power from methane (fed at a 2 kmol/h rate) can now be heat and power integrated, so as to accurately assess when is energetic self-sufficiency attainable for the proposed reaction cluster realization. The two cases are again considered: the co-production of acetic acid and hydrogen, Case 1, and the co-production of acetic acid and power, $Y = 0$, Case 2. The heat and power integration process closely follows that outlined in [46, 47]. This globally optimal thermodynamic heat and power integration approach seeks to determine the minimum total hot/cold/electric utility cost necessary to achieve the desired energy changes associated with given process streams with known flow rates, inlet and outlet temperatures and utility (hot/cold) streams with known inlet and outlet temperatures [46]. Both streams with sensible and latent heat supply/demand requirements are considered. To ensure compliance with energetic self-sufficiency, only a cold utility at 298 K is allowed. The work/cold utility cost ratio is 29/105, while the downward (hot stream) and upward (cold stream) minimum approach temperatures are 5 K. The heat and power integration process is repeated for converged flow sheets corresponding to both case 1, and case 2 (Y = 0), and to different values of the oxygen/acetic acid molar ratio, X in the range $0 \le X \le 2$.

Figure 14 shows a plot of net work of the process with respect to X for both case 1, and case 2 (Y = 0). For case 1, energetic self-sufficiency occurs when $1.295 \le X \le 2$, while for case 2 (Y = 0), energetic self-sufficiency occurs when $0 \le X \le 2$. The work generation resulting from each heat and power integration study, is obtained considering that the abstract heat engine/pump operations employed are isentropic. The hydrogen combustion turbine subsystem is also considered to be

100% efficient. Thus, to properly access real power generation/consumption, the heat and power integration and hydrogen combustion turbine work numbers are adjusted to reflect a common efficiency used throughout the study of 75%.

From figure 14, it is easy to identify that the power generated by the case 1 design increases, i.e. becomes more negative as X increases. On the other hand, the power generated by the case 2, Y = 0 design increases, i.e., becomes more negative, for $0 \le X \le 1.2$, and decreases, i.e., becomes less negative, for $1.2 \le X \le 2$.

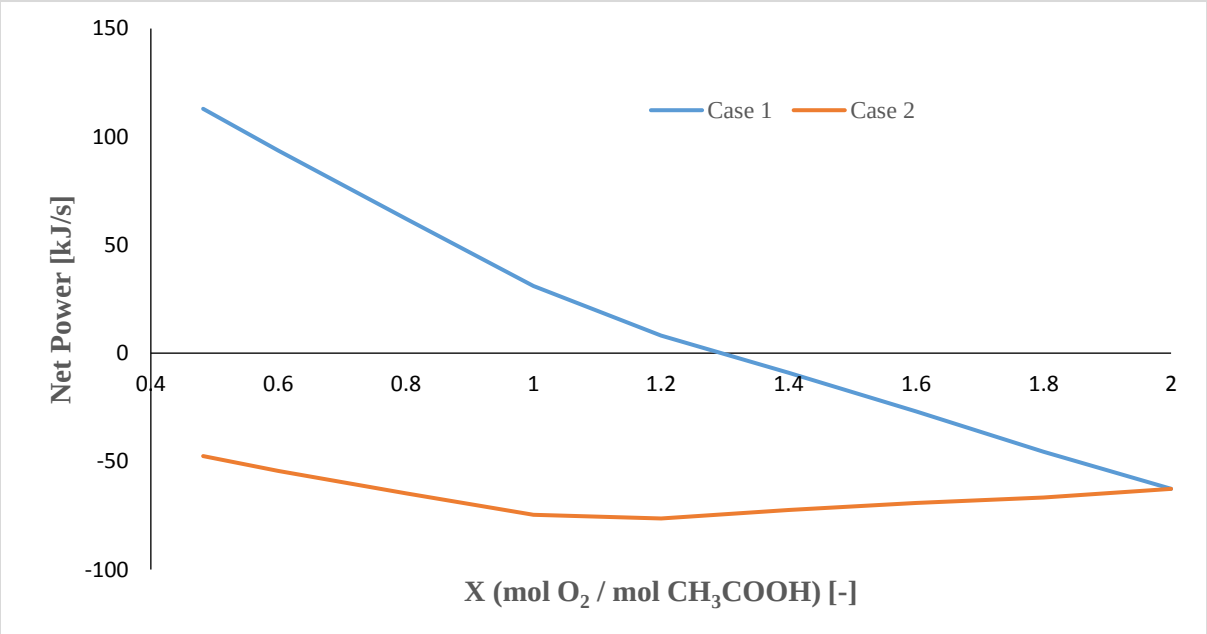

Figure 14: Net power generation vs. X for cases 1 and 2 (Y = 0) (per 2 kmol/h methane feed)

Two design points, $X = 1.238$ and $X = 0.482$ are selected to demonstrate the economic potential of the proposed process. The selected operating points for case 1 and case 2 (Y = 0) are shown on the $X - \dot{S}_G$ space in figure 15.

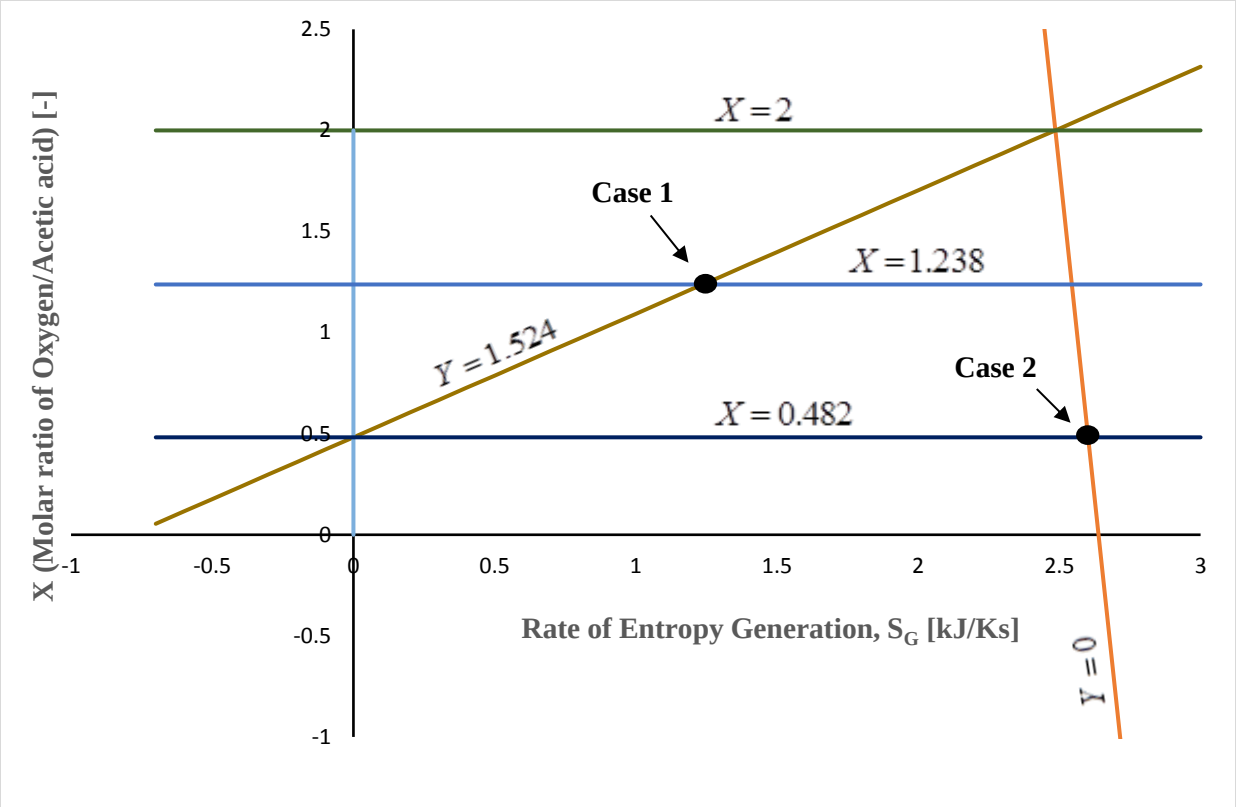

Figure 15: Case 1, Case 2 (Y = 0) designs in energetic self-sufficiency feasible region in (X, S_G) space

Figure 16 shows the temperature-entropy (T-S) diagram of the heat and power integrated flowsheet at $X = 1.238$. At this operating point, the process requires three heat engines and two heat pumps to satisfy the energy requirements of the flowsheet. Figure 17 shows the temperature-entropy (T-S) diagram of the heat and power integrated flowsheet at $X = 0.482$. At this operating point, the process requires three heat engines and two heat pumps to satisfy the energy requirements of the flowsheet. Comparison of the two diagrams demonstrates that the heat pumping region is much more substantive in temperature span in the latter design. This is consistent with the much higher power consumption within the proposed subsystem Ω for the $X = 0.482$ design, as compared to the small power generation of subsystem Ω for the $X = 1.238$ design. In contrast, when

subsystem Ω is combined with the hydrogen combustion turbine subsystem, the overall systems total power generation is higher for the $X = 0.482$ as compared to the $X = 1.238$ design. This is attributable to the large power generation in the hydrogen combustion turbine subsystem for the $X = 0.482$ as compared to the $X = 1.238$ design, due to the significantly higher amount of hydrogen generated in the former design.

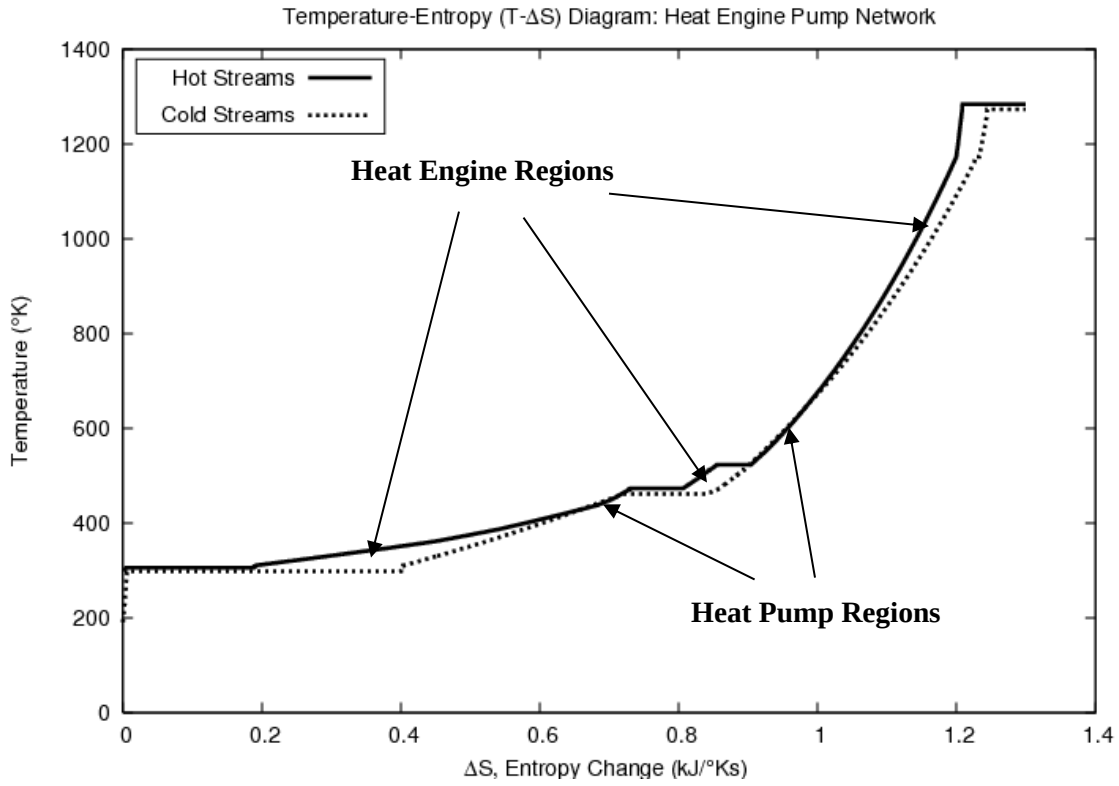

Figure 16: Temperature-Entropy (T-S) diagram of the Heat Engine/Pump Network at X = 1.238

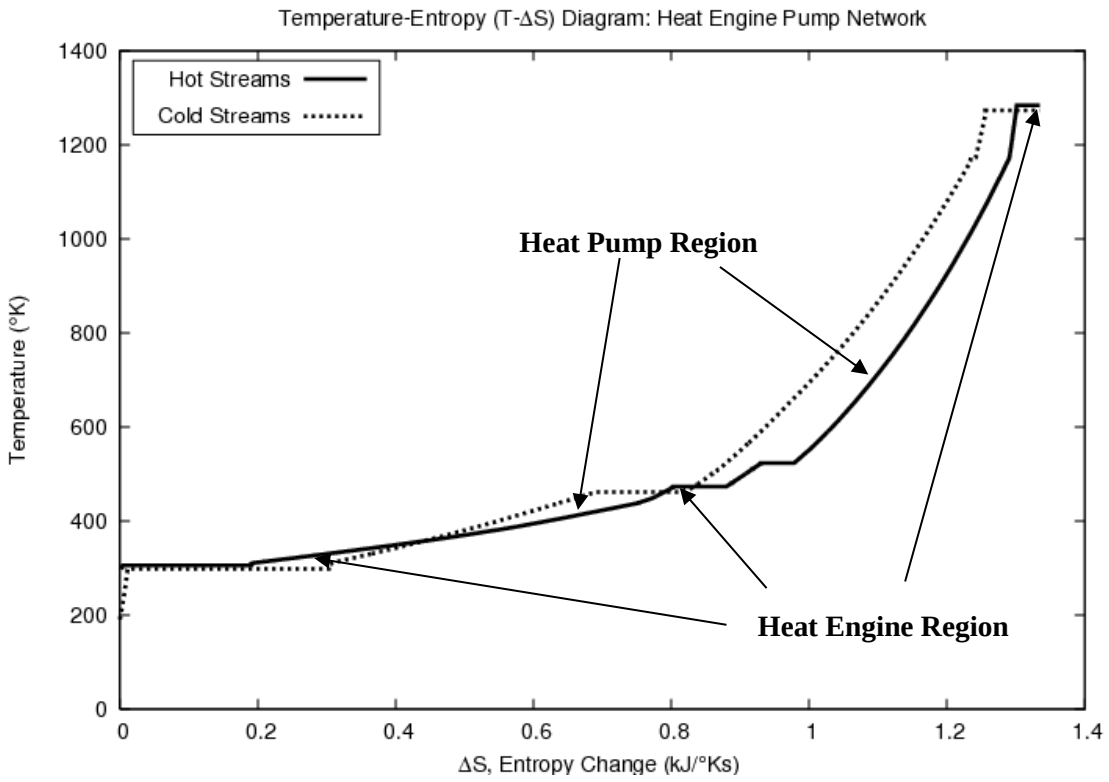

Figure 17: Temperature-Entropy (T-S) diagram of the Heat Engine/Pump Network at X = 0.482

7. ECONOMIC ANALYSIS AND PROFITABILITY

A preliminary economic analysis is carried out on the proposed natural gas to acetic acid and hydrogen/power process. For comparison purposes, a preliminary economic analysis of a natural gas combustion, Carnot engine subsystem is also carried out. For the proposed process, Case 1 is analyzed at an oxygen/acetic acid molar ratio of 1.238 and case 2 (Y = 0) is analyzed at an oxygen/acetic acid molar ratio of 0.482. The overall reactions for both cases respectively are:

$$2CH_4^{(g)} + 1.238O_2^{(g)} \rightarrow CH_3COOH^{(aq)} + 1.524H_2^{(g)} + 0.476\ H_2O^{(l)} \qquad (R17)$$

$$2CH_4^{(g)} + 2O_2^{(g)} \rightarrow CH_3COOH^{(aq)} + 2\ H_2O^{(l)} \qquad (R18)$$

In the heat and power integration analysis of the previous section, the abstract heat engine/pump operations are considered isentropic, while the specific turbine/compressor/pumping operations employed in the flowsheet feature 75% adiabatic efficiencies. Isentropic work generation operations are also employed in the hydrogen combustion turbine subsystem, and in the Carnot engine subsystem of the natural gas combustion system used for comparison purposes. Thus, to properly assess the real work generation/consumption of these abstract operations, especially for economic purposes, an efficiency of 75% is imposed on all work values obtained using an isentropic ideal operation assumption (i.e. heat and power integration of proposed process subsystem; hydrogen combustion turbine subsystem; natural gas combustion/Carnot engine alternative design).

The cost of the oxygen supplied to the presented flowsheets can be estimated by quantifying the energy cost associated with the generation of high purity oxygen through air separation. This is reflected in the economic analysis, by considering the work of oxygen separation which is 48,000

kJ per kmol of oxygen produced [48]. All other power consumption (pumps, compressors, etc.) is reflected in the flowsheet's net power generation calculations.

7.1 Operating Cost Analysis

7.1.1 *Case 1: Acetic Acid and Hydrogen*

For case 1, Table 3 gives the overall profit margin accruable from the process. The operating costs include natural gas (methane) purchases and power consumption for oxygen separation. The operating revenue includes the sale of acetic acid and hydrogen. The profit margin amounts to $30.348/h per 32.08 kg/h feed of methane, translating to $0.946/h per 1 kg/h of methane feed.

Table 3: Operating cost analysis of process co-producing acetic acid and hydrogen (Case 1) at an oxygen/acetic acid molar ratio of 1.238.

	Unit Cost	Unit	Unit Cost Ref.	Net Amount Consumed	Unit	Total	Unit
EXPENDITURE							
Natural Gas	0.298	($/kg)	[13]	32.08	kg/h	9.560	($/h)
O_2 Production Power Consumption	0.105	($/kWh)	[13]	16.50	kW	1.733	($/h)
				Total Expenditure:		**11.292**	**($/h)**
	Unit Cost	**Unit**	**Unit Cost Ref.**	**Net Amount Produced**	**Unit**	**Total**	**Unit**
REVENUE							
Acetic acid	0.5	($/kg)	[49]	60.05	kg/h	30.025	($/h)
Hydrogen	3.64	($/kg)	[15]	3.191	kg/h	11.615	($/h)

Total Revenue:	**41.640**	**($/h)**
Profit Margin:	**30.348**	**($/h)**

7.1.2 *Case 2: Acetic Acid and Power generation*

Similarly, the economic analysis for case 2 (Y = 0) is presented in Table 4. The operating costs are identical to case 1, while the operating revenues include acetic acid and net power sales. The profit margin for this scenario amounts to $22.66/h per 32.08 kg/h feed of methane, which translates to a profit of $0.706/h per 1 kg/h of methane feed.

Table 4: Operating cost analysis of process co-producing acetic acid and power (Case 2, Y = 0) at an oxygen/acetic acid molar ratio of 0.482.

	Unit Cost	**Unit**	**Unit Cost Ref.**	**Net Amount Consumed**	**Unit**	**Total**	**Unit**
EXPENDITURE							
Natural Gas	0.298	($/kg)	[13]	32.08	kg/h	9.560	($/h)
O_2 Production Power Consumption	0.105	($/kWh)	[13]	26.66	kW	2.799	($/h)
					Total Expenditure:	**12.359**	**($/h)**
	Unit Cost	**Unit**	**Unit Cost Ref.**	**Net Amount Produced**	**Unit**	**Total**	**Unit**
REVENUE							
Acetic acid	0.5	($/kg)	[49]	60.05	kg/h	30.025	($/h)
Net Power Produced	0.105	($/kWh)	[13]	47.56	kW	4.994	($/h)

Total Revenue:	**35.019**	**($/h)**
Profit Margin:	**22.660**	**($/h)**

The above suggests that the operating profit for the case 1 design is 34% higher than the operating profit for the (case 2, Y = 0) design. For both cases, the greatest revenue stream comes from the sale of acetic acid, making apparent the economic importance of eliminating carbon dioxide emissions by redirecting the contained carbon into a saleable product.

It is instructive to compare these operating profits to a conventional Natural Gas Combined Cycle (NGCC) power plant consuming natural gas and generating power (R19) by first considering an ideal Carnot cycle, and then imposing an 75% adiabatic efficiency. The Carnot cycle is operated between a hot utility of 1273 K and a cold utility of 298 K, values which correspond to the temperatures employed in the acetic acid process subsystem's incomplete combustion (IC) reaction and cold utility respectively. The resulting Carnot efficiency is 76.6%, which is then further reduced to 57.5% by imposing a 75% efficiency on the Carnot cycle's turbine/pump operations. From eqn. (10), the power produced by the NGCC plant is 285.22 kW. The operating cost of this NGCC plant includes natural gas (methane) purchases while the revenue includes the sale of power produced. This yields a profit of $20.39/h per 32.08 kg/h feed of methane or $0.636/h per 1 kg/h methane feed. When carbon capture is incorporated in the NGCC power plant, a typical efficiency penalty of 14.7% for 90% carbon capture is incurred [50]. This results in an efficiency of 49% and a profit of $15.96/h per 32.08 kg/h feed of methane or $0.498/h per 1 kg/h methane feed.

$$CH_4^{(g)} + 2O_2^{(g)} \rightarrow CO_2^{(g)} + 2H_2O^{(l)} \qquad \Delta h_r^o(298) = -55,665.6\ kJ/kg\,CH_4 \qquad (R19)$$

$$\Delta h_r^o(298) = -55,665.6\ kJ/kg\ CH_4 \times \frac{32.08}{3600}\ kg/s\ CH_4 = -496.04[kW]$$

$$W_{net(NGCC)} = 0.575(-496.04) = -285.22[kW] \quad (10)$$

The operating profits of case 1 and case 2 (Y = 0) are higher by 90% and 42% respectively than the operating profit of a NGCC power plant with 90% carbon capture.

7.2 Capital Cost Analysis

A capital cost analysis is presented in this section to give a preliminary estimate of the capital cost for the construction of the proposed acetic acid plant. A typical Natural Gas Combined Cycle (NGCC) power plant as reported in [50, 51] with key data summarized in Table 5, is used as a basis of comparison and for the costing of some major equipment utilized in the acetic acid process.

Table 5: Baseline NGCC Power Plant Basic Data

	Operating Conditions	Amount	Ref
Natural Gas Combined Cycle (NGCC)	Natural Gas feed flowrate	70,663 kg/h *	[50]
	Net Power Output	473.57 MWe	[51]
	Total amount of CO_2 captured via a 90% carbon capture scenario	182, 203 kg/hr	
	Capital Cost	**$ 715, 450, 000.00**	

**For simplicity of comparison, it has been assumed here that the natural gas consists entirely of methane.*

For equal comparison, the acetic acid plant, at an oxygen/acetic acid molar ratio of 0.482, must receive the same amount of natural gas feed as the NGCC plant. A new converged flowsheet reflecting this new natural gas feed flow rate is developed and the major equipment list for the process as well as the total cost estimate is shown in Table 6. Cost is based on 2011-dollar basis and the final cost is scaled using the Nelson-Farrer (NF) Refinery Construction Index.

Table 6: Capital Cost Estimate - Major equipment list and associated cost at X = 0.482.

Equipment	Unit Name	Total Capacity for cost estimate	Total Cost	Ref	Notes
Compressors	CH_4 compressors	15, 960 kW	$ 18, 153, 814.85	[52]	a, b
	CO compressors	4, 520 kW	$ 19, 398, 439.69		
	H_2 compressor	3, 434 kW	$ 8, 098, 466.56		
	Syngas Compressor (for Methanol Synthesis)	6, 166 kW	$ 10, 893, 277.89		
	Distillation Column Recycle Compressor	1, 137 kW	$ 4, 878, 315.16		
		Sub-Total	**$ 61, 422, 314.15**		
Pumps	SMR feedwater Pump	99.54 m^3/h; 95 kW	$ 105, 072.22	[52]	a, b
	Recycled water Pump	24.48 m^3/h; 23 kW	$ 52, 679.13		
		Sub-Total	**$ 157, 751.35**		

Turbines	Hydrogen Expander	6, 744 kW	$ 3, 514, 990.01		
	Hydrogen Combustion turbine	351, 466 kW	$ 44, 600, 005.86	[52]	a, b
		Sub-Total	**$ 48, 114, 995.87**		
Separators	IC Product	375, 849 kg shell mass	$ 2, 831, 485.79		
	Syngas Flash	612, 014 kg shell mass	$ 3, 793, 698.22	[52]	a, b, c, k
	RWGS Flash	16, 519, 241 kg shell mass	$ 27, 403, 121.40		
	H_2 + H_2O Flash	612, 014 kg shell mass	$ 3, 793, 698.22		
		Sub-Total	**$ 37, 822, 003.63**		
Reactors	Incomplete Combustion Reactor	45, 070 kg/h feed flow rate	$ 4, 077, 784.96	[50] [51]	d, k
	Steam Methane Reformer	301, 100 kg/h feed flow rate	$ 71, 807, 190.45	[13]	e, k
	RWGS Reactor	1, 595, 000 kg/h feed flow rate	$ 34, 653, 587.18	[50] [51]	d, k

	Methanol Synthesis Reactor	233, 300 kg/h feed	$ 4, 029, 9390.91	[40]	f, k
	Acetic Acid Reactor	24, 898, 750 kg/h feed flow rate	$ 66, 413, 468.91	[40]	f, k
		Sub-Total	**$ 180, 981, 970.59**		
Distillation Column	Distillation Column	3, 384, 553.55 kg shell mass	$ 17, 218, 830.53	[52]	a, b, g, k
		Sub-Total	**$ 17, 218, 830.53**		
Pressure Swing Adsorbers, H_2 Separator and CO_2 Adsorption Unit	Air Separation PSA	604, 227 kg/hr air feed flow rate	$ 240, 521, 448.80	[50] [51]	h, k
	H_2 Membrane Separator	147, 500 kg/hr feed flow rate	$ 99, 619, 084.01	[13]	i, k
	CO_2 Adsorption Unit	1, 700, 000 kg/hr feed flow rate	$ 398, 000, 993.21		j, k
		Sub-Total	**$ 738, 141, 526.02**		

Heat Exchangers	Heat Exchangers	5, 557 m^2 total area; 202.38 MW (heat and power integration)	$ 83, 002, 463.09	[46] [55] [56]	b, l
		Sub-Total	**$ 83, 002, 463.09**		
Generic costs	Accessory Electric Plant	Net power output of 104.16 MWe at X = 0.482	$ 22, 101, 558.00	[50] [51]	m, k
	Instrumentation and Control		$ 7, 321, 224.00		
	Improvements to site		$ 4, 456, 974.00		
	Building and Structures		$ 4, 843, 296.00		
		Sub-Total	**$ 38, 723,052.00**		
		Grand Total	**$ 1, 205, 584, 907.23**		

Notes

a) Cost-of-equipment is based on preliminary cost estimate procedures found in [52].

b) The factored estimation methodology [53] is used to arrive at a total cost estimate with distributive factors for bulk materials based on the cost of equipment.

c) The shell mass is calculated using the vessel sizing utility of UNISIM.

d) Cost is based on the WGSR reactor feed flowrate and cost of the WGSR reactor as specified in [50, 51].

e) Cost is based on SMR reactor feed flowrate and cost of the SMR specified in [13].

f) Cost is based on High Pressure (HP) methanol reactor feed flowrate and the cost of the HP methanol synthesis reactor specified in [40].

g) Size of tray sections is estimated using the tray sizing utility of UNISIM. Valve tray cost is included in final cost.

h) Cost is based on air PSA feed flowrate and cost of the air separation unit specified in [50, 51].

i) Cost is based on hydrogen PSA feed flowrate and the cost of the H_2-PSA specified in [13].

j) Cost is based on syngas feed flowrate to a typical amine based CO_2 capture system and the reported cost of the system as specified in [13].

k) Final cost estimate is determined by using the six-tenths factor rule [54].

l) The heat exchange area is estimated using principles found in [55, 56]. The cost estimate also includes the energy requirement of any heat pump/engine, which is determined from heat and power integration analysis of the flowsheet [46].

m) Cost is based on net power produced and the cost of the various modules specified in [50, 51].

8. DISCUSSION-CONCLUSIONS

A novel process for the co-production of acetic acid and hydrogen/power from natural gas with zero carbon dioxide emissions was developed. Two cases were explored – the co-production of acetic acid and hydrogen (Case 1) and the co-production of acetic acid and power (Case 2). In addition to zero carbon dioxide emissions, the novel designs proposed in this work are always energetically self-sufficient for case 2 (Y = 0) and for case 1 within the range $1.295 \leq X \leq 2$. Operating points of $X = 1.238$ and $X = 0.482$ are chosen to demonstrate the economic potential of the proposed process for case 1 and case 2 (Y = 0) respectively. The energy requirements of the flow sheet for both cases are each met by 3 heat engines and 2 heat pumps. A preliminary economic analysis reveals an increase in the operating profit by 90% (Case 1) and 42% (Case 2, Y = 0) respectively, compared to a typical natural gas combined cycle (NGCC) power plant (with 90% carbon capture) fed with the same amount of natural gas.

To assess the carbon capture potential and other metrics of the proposed plant, a cost and performance metric calculation, defined in [16], is carried out on the plant. The acetic acid plant is assessed on CO_2 utilization efficiency, CO_2 utilization potential, CO_2 utilization intensity and Product marketability. The calculations are based on the maximum amount of CO_2 obtainable from the natural gas (methane) feed to the process and this is adjudged to stem from the complete combustion of natural gas in a typical NGCC power plant (Table 5). The acetic acid process produces as valuable products, 131, 500 kg/h (1.152 million tons/year) of acetic acid and 6, 729 kg/h (0.059 million tons/year) of hydrogen (case 1) or 104.16 MWe net power (case 2).

a) CO_2 Utilization Efficiency

$$CO_2\ Utilization\ Efficiency\,(\%) = \frac{tonnes\ CO_2\ utilized}{tonnes\ CO_2\ \ fed\ to\ process} \times 100$$

$$CO_2\ Utilization\ Efficiency\,(\%) = \frac{1.77\ million\ tonnes\ /\ yr}{1.77\ million\ tonnes\ /\ yr} \times 100 = 100\%$$

The acetic acid plant has a CO_2 utilization efficiency of 100% as it generates no carbon dioxide emissions. This is more than the 90% CO_2 capture (utilization) efficiency currently obtainable from current SOTA carbon capture techniques [13, 50, 57].

b) CO_2 Utilization Potential

The world market demand of acetic acid is 12.1 million tons per year (2014 basis) [4]. Considering that this worldwide production originates from natural gas using the proposed process, suggests a worldwide natural gas consumption of 6.4 million tons per year (17.75 million tons per year CO_2). The amount of CO_2 available from a reference single typical NGCC power plant is 182, 203 kg/h (1.596 million tons per year) [50].

$$CO_2\ Utilization\ Potential = \frac{tonnes\ /\ yr\ \ CO_2\ utilized\ to\ meet\ market\ demand}{tonnes\ /\ yr\ \ CO_2\ available\ \ from\ a\ reference\ plant}$$

$$CO_2\ Utilization\ Potential = \frac{17.75}{1.596} \times 100\% = 1{,}112\%$$

c) CO_2 Utilization Intensity

The potential amount of CO_2 utilized is the amount that would have been generated from the consumption of natural gas, which is 1.467 million tons per year CO_2 per million ton of acetic acid produced.

$$CO_2\ Utilization\ Intensity\left(\%\right)=\frac{tonnes/\ yr\ CO_2\ utilized}{tonnes\ product\ produced}\times100$$

$$CO_2\ Utilization\ Intensity\left(\%\right)=\frac{1.467}{1}\times100=146.7\%$$

d) Product Marketability

The cost to make a ton of acetic acid and the corresponding amount of hydrogen is calculated from the total operating cost of Case 1 to be $188/ton of acetic acid (Table 3). The revenues that can be obtained from sales of acetic acid and hydrogen are $ 500/ton [49] and $ 3, 640/ton [15] respectively.

$$Product\ Marketability\left(\%\right)=\frac{\$\ cost\ to\ make\ a\ tonne\ of\ \ desired\ \ product}{\$\ per\ tonne\ market\ value\ of\ \ desired\ \ product}\times100$$

$$Product\ Marketability\left(\%\right)=\frac{\$188}{\$4{,}140}\times100=4.54\%$$

In summary, the proposed process is beneficial at many levels. It redirects the carbon contained in the natural gas feed, which would normally be emitted as carbon dioxide into the atmosphere, into a saleable product, namely acetic acid, whose sales improve overall plant economics. The proposed process is also energetically self-sufficient for a wide range of the molar ratio X of oxygen to acetic acid ($1.295\le X\le2$ for case 1 and $0\le X\le2$ for case 2, Y = 0). A preliminary economic analysis indicates that the proposed process features 90% (Case 1) and 42% (Case 2, Y = 0) respectively higher operating profits than those of a natural gas combined cycle (NGCC) power plant with 90% carbon capture. It also features a payback period of 2 and 3 years for case 1 (X =

1.238) and case 2 (X = 0.482, Y = 0) respectively, which is comparable to the 2.5 years payback period for a conventional NGCC plant.

REFERENCES

[1] Agreda, V. H. (Ed.). (1992). *Acetic acid and its derivatives*. CRC Press.

[2] Yoneda, N., Kusano, S., Yasui, M., Pujado, P., & Wilcher, S. (2001). Recent advances in processes and catalysts for the production of acetic acid. *Applied Catalysis A: General*, *221*(1), 253-265.

[3] Le Berre, C., Serp, P., Kalck, P., & Torrence, G.P. (2013). Acetic Acid. *Ullmann's Encyclopedia of Industrial Chemistry*.

[4] http://www.prnewswire.com/news-releases/global-acetic-acid-market---segmented-by-application-and-geography---trends-and-forecasts-2015-2020---reportlinker-review-300145381.html, September, 2015.

[5] https://www.grandviewresearch.com/press-release/global-acetic-acid-market, February, 2014.

[6] Huang, W., Zhang, C., Yin, L., & Xie, K. (2004). Direct Synthesis of Acetic Acid from CH_4 and CO_2 in the Presence of O_2 over a V_2O_5-$PdCl_2/Al_2O_3$ Catalyst. *Journal of Natural Gas Chemistry*, *13*, 113-115.

[7] Jones, J. H. (2000). The Cativa^{TM} process for the manufacture of acetic acid. *Platinum Metals Review*, *44*(3), 94-105.

[8] Howard, M. J., Jones, M. D., Roberts, M. S., & Taylor, S. A. (1993). C1 to acetyls: catalysis and process. *Catalysis Today*, *18*(4), 325-354.

[9] Sunley, G. J., & Watson, D. J. (2000). High productivity methanol carbonylation catalysis using iridium: the Cativa™ process for the manufacture of acetic acid. *Catalysis Today*, *58*(4), 293-307.

[10] Haynes, A., Maitlis, P. M., Morris, G. E., Sunley, G. J., Adams, H., Badger, P. W., Bowers, C. M., Cook, D. B., Elliot, P. I. P., Ghaffar, T., Green, H., Griffin, T. R., Payne, M., Pearson, J. M., Taylor, M. J., Vickers, P. W., & Watt, R. J. (2004). Promotion of iridium-

catalyzed methanol carbonylation: Mechanistic studies of the Cativa process. *Journal of the American Chemical Society*, *126*(9), 2847-2861.

[11] Haussinger, P., Lohmuller, R., & Watson, A.M. (2012). Hydrogen, 6. Uses. *Ullmann's Encyclopedia of Industrial Chemistry*.

[12] Energy Information Administration. US Dry Natural Gas Production, August 2016.

[13] Rath, L. K. (2010). Assessment of hydrogen production with CO_2 capture volume 1: Baseline state-of-the-art plants. *DoE/NETL, report, 1434*.

[14] McFarlan, A. J. (1997). *U.S. Patent No. 5,659,077*. Washington, DC: U.S. Patent and Trademark Office.

[15] Lopez, J. A. P., & Manousiouthakis, V. I. (2011). Natural gas based hydrogen production with zero carbon dioxide emissions. *International Journal of Hydrogen Energy*, *36*(20), 12853-12868.

[16] Black, J. (2014). Cost and Performance metrics used to assess Carbon Utilization and Storage Technologies. Final report. DOE/NETL-341/093013.

[17] Abbott, M. M., Smith, J. M., & Van Ness, H. C. (2001). Introduction to Chemical Engineering Thermodynamics. *McGraw-Hill, Boston*, 619-626.

[18] Haynes, W. M. (Ed.). (2014). *CRC handbook of chemistry and physics*. CRC press.

[19] Rudd, D. F., Powers, G. J., & Siirola, J. J. (1973). *Process synthesis*. Englewood Cliffs, NJ: Prentice-Hall.

[20] May, D., & Rudd, D. F. (1976). Development of solvay clusters of chemical reactions. *Chemical Engineering Science, 31*(1), 59-69.

[21] Rotstein, E., Resasco, D., & Stephanopoulos, G. (1982). Studies on the synthesis of chemical reaction paths—I: Reaction characteristics in the (ΔG, T) space and a primitive synthesis procedure. *Chemical Engineering Science, 37*(9), 1337-1352.

[22] Holiastos, K., & Manousiouthakis, V. (1998). Automatic synthesis of thermodynamically feasible reaction clusters. *AIChE journal, 44*(1), 164-173.

[23] Pena, M. A., Gomez, J. P., & Fierro, J. G. (1996). New catalytic routes for syngas and hydrogen production. *Applied Catalysis A: General, 144*(1), 7-57.

[24] Meerman, J. C., Hamborg, E. S., Van Keulen, T., Ramírez, A., Turkenburg, W. C., & Faaij, A. P. C. (2012). Techno-economic assessment of CO_2 capture at steam methane reforming facilities using commercially available technology. *International journal of greenhouse gas control, 9*, 160-171.

[25] Armor, J. N. (1999). The multiple roles for catalysis in the production of H_2. *Applied Catalysis A: General, 176*(2), 159-176.

[26] Tindall, B. M., & King, D. L. (1994). Designing steam reformers for hydrogen production. *Hydrocarbon Processing;(United States), 73*(7).

[27] Rajesh, J. K., Gupta, S. K., Rangaiah, G. P., & Ray, A. K. (2001). Multi-objective optimization of industrial hydrogen plants. *Chemical Engineering Science, 56*(3), 999-1010.

[28] Kaiser, P., Unde, R. B., Kern, C., & Jess, A. (2013). Production of Liquid Hydrocarbons with CO_2 as Carbon Source based on Reverse Water-Gas Shift and Fischer-Tropsch Synthesis. *Chemie Ingenieur Technik, 85*(4), 489-499.

[29] Wolf, A., Jess, A., & Kern, C. (2016). Syngas Production via Reverse Water-Gas Shift Reaction over a Ni-Al_2O_3 Catalyst-Catalyst Stability, Reaction Kinetics and Reactor Modeling. *Chemical Engineering & Technology 39(*6), 1040-1048.

[30] Daza, Y. A., & Kuhn, J. N. (2016). CO_2 conversion by reverse water gas shift catalysis: comparison of catalysts, mechanisms and their consequences for CO_2 conversion to liquid fuels. *RSC Advances, 6*(55), 49675-49691.

[31] Yun, S., & Oyama, S. T. (2011). Correlations in palladium membranes for hydrogen separation: a review. *Journal of membrane science, 375*(1), 28-45.

[32] Harale, A., Hwang, H. T., Liu, P. K., Sahimi, M., & Tsotsis, T. T. (2007). Experimental studies of a hybrid adsorbent-membrane reactor (HAMR) system for hydrogen production. *Chemical Engineering Science, 62*(15), 4126-4137.

[33] Yong, Z., Mata, V., & Rodrigues, A. E. (2002). Adsorption of carbon dioxide at high temperature—a review. *Separation and Purification Technology, 26*(2), 195-205.

[34] Öztürk, S. S., Shah, Y. T., & Deckwer, W. D. (1988). Comparison of gas and liquid phase methanol synthesis processes. *The Chemical Engineering Journal, 37*(3), 177-192.

[35] Riaz, A., Zahedi, G., & Klemeš, J. J. (2013). A review of cleaner production methods for the manufacture of methanol. *Journal of Cleaner Production, 57*, 19-37.

[36] Ott, J., Gronemann, V., Pontzen, F., Fiedler, E., Grossmann, G., Kersebohm, D. B., Weiss, G. & Witte, C. (2012). Methanol. *Ullmann's Encyclopedia of Industrial Chemistry*.

[37] Lange, J. P. (2001). Methanol synthesis: a short review of technology improvements. *Catalysis Today, 64*(1), 3-8.

[38] Bartholomew, C. H., & Farrauto, R. J. (2006). Hydrogen production and synthesis gas reactions. *Fundamentals of Industrial Catalytic Processes, Second Edition*, 339-486.

[39] De Klerk, A. (2012, January). Gas-to-liquids conversion. In *Natural Gas Conversion Technologies Workshop. Houston: US Department of Energy*.

[40] Phillips, S. D., Tarud, J. K., Biddy, M. J., & Dutta, A. (2011). *Gasoline from wood via integrated gasification, synthesis, and methanol-to-gasoline technologies* (No. NREL/TP-5100-47594). National Renewable Energy Laboratory (NREL), Golden, CO.

[41] Raudaskoski, R., Turpeinen, E., Lenkkeri, R., Pongrácz, E., & Keiski, R. L. (2009). Catalytic activation of CO_2: use of secondary CO_2 for the production of synthesis gas and for methanol synthesis over copper-based zirconia-containing catalysts. *Catalysis Today, 144*(3), 318-323.

[42] Lee, S. (1990). Methanol synthesis technology. CRC Press.

[43] Haynes, A. (2006). Acetic acid synthesis by catalytic carbonylation of methanol. In *Catalytic Carbonylation Reactions* (pp. 179-205). Springer Berlin Heidelberg.

[44] Bannister, R. L., Newby, R. A., & Yang, W. C. (1998). Development of a hydrogen-fueled combustion turbine cycle for power generation. *Journal of engineering for gas turbines and power, 120*(2), 276-283.

[45] Honeywell. UniSim® thermo reference guide, 2008.

[46] Holiastos, K., & Manousiouthakis, V. (2002). Minimum hot/cold/electric utility cost for heat exchange networks. *Computers & chemical engineering, 26*(1), 3-16.

[47] Posada, A., & Manousiouthakis, V. (2005). Heat and power integration of methane reforming based hydrogen production. *Industrial & engineering chemistry research, 44*(24), 9113-9119.

[48] Ruthven, D. M., Farooq, S., & Knaebel, K. S. (1994). *Pressure swing adsorption* (Vol. 480). New York: VCH publishers.

[49] Tecnon OrbiChem, Chemical Market Insight and foresight – on a single page, Acetic Acid, 2013.

[50] Black, J. (2010). Cost and performance baseline for fossil energy plants volume 1: Bituminous coal and natural gas to electricity. *National Energy Technology Laboratory: Washington, DC, USA*.

[51] Woods, M., Pinkerton, L. R., & Varghese, E. (2012). Updated Costs (June 2011 Basis) for Selected Bituminous Baseline Cases. *Washington, DC: DOE/NETL, 49*.

[52] Towler, G., & Sinnott, R. K. (2012). *Chemical engineering design: principles, practice and economics of plant and process design*. Elsevier.

[53] Loh, H. P., Lyons, J., & White, C. W. (2002). Process equipment cost estimation. Final Report, National Energy Technology Center.

[54] Peters, M. S., Timmerhaus, K. D., West, R. E., Timmerhaus, K., & West, R. (1968). *Plant design and economics for chemical engineers* (Vol. 4). New York: McGraw-Hill.

[55] Linnhoff, B., & Ahmad, S. (1990). Cost optimum heat exchanger networks—1. Minimum energy and capital using simple models for capital cost. *Computers & Chemical Engineering*, *14*(7), 729-750.

[56] Manousiouthakis, V., & Martin, L. L. (2004). A minimum area (MA) targeting scheme for single component MEN and HEN synthesis. *Computers & chemical engineering*, *28*(8), 1237-1247.

[57] Ciferno, J. P., Ramezan, M., Skone, T. J., Nsakala, N. Y., Liljedahl, G. N., Gearhart, L. E., Hestermann, R., & Rederstorff, B. (2007). Carbon dioxide capture from existing coal-fired power plants. *National Energy Technology Laboratory, DOE/NETL Report*, (401/110907).